Journal of Sedimentary Research

Journal of Sedimentary Research, 2021, v. 91, 1–25
Research Article
DOI: 10.2110/jsr.2021.004

A LITHOFACIES ANALYSIS OF A SOUTH POLAR GLACIATION IN THE EARLY PERMIAN: PAGODA FORMATION, SHACKLETON GLACIER REGION, ANTARCTICA

LIBBY R.W. IVES AND JOHN L. ISBELL

University of Wisconsin–Milwaukee, Department of Geosciences, Lapham Hall, 3209 North Maryland Avenue, Milwaukee, Wisconsin 53211, U.S.A.
e-mail: woodfor5@uwm.edu

ABSTRACT: **The currently favored hypothesis for Late Paleozoic Ice Age glaciations is that multiple ice centers were distributed across Gondwana and that these ice centers grew and shank asynchronously. Recent work has suggested that the Transantarctic Basin has glaciogenic deposits and erosional features from two different ice centers, one centered on the Antarctic Craton and another located over Marie Byrd Land. To work towards an understanding of LPIA glaciation that can be tied to global trends, these successions must be understood on a local level before they can be correlated to basinal, regional, or global patterns. This study evaluates the sedimentology, stratigraphy, and flow directions of the glaciogenic, Asselian–Sakmarian (Early Permian) Pagoda Formation from four localities in the Shackleton Glacier region of the Transantarctic Basin to characterize Late Paleozoic Ice Age glaciation in a South Polar, basin-marginal setting. These analyses show that the massive, sandy, clast-poor diamictites of the Pagoda Fm were deposited in a basin-marginal subaqueous setting through a variety of glaciogenic and glacially influenced mechanisms in a depositional environment with depths below normal wave base. Current-transported sands and stratified diamictites that occur at the top of the Pagoda Fm were deposited as part of grounding-line fan systems. Up to at least 100 m of topographic relief on the erosional surface underlying the Pagoda Fm strongly influenced the thickness and transport directions in the Pagoda Fm. Uniform subglacial striae orientations across 100 m of paleotopographic relief suggest that the glacier was significantly thick to "overtop" the paleotopography in the Shackleton Glacier region. This pattern suggests that the glacier was likely not alpine, but rather an ice cap or ice sheet. The greater part of the Pagoda Fm in the Shackleton Glacier region was deposited during a single retreat phase. This retreat phase is represented by a single glacial depositional sequence that is characteristic of a glacier with a temperate or mild subpolar thermal regime and significant meltwater discharge. The position of the glacier margin likely experienced minor fluctuations (readvances) during this retreat. Though the sediment in the Shackleton Glacier region was deposited during a single glacier retreat phase, evidence from this study does not preclude earlier or later glacier advance–retreat cycles preserved elsewhere in the basin. Ice flow directions indicate that the glacier responsible for this sedimentation was likely flowing off of an upland on the side of the Transantarctic Basin closer to the Panthalassan–Gondwanide margin (Marie Byrd Land), which supports the hypothesis that two different ice centers contributed glaciogenic sediments to the Transantarctic Basin. Together, these observations and interpretations provide a detailed local description of Asselian–Sakmarian glaciation in a South Polar setting that can be used to understand larger-scale patterns of regional and global climate change during the Late Paleozoic Ice Age.**

INTRODUCTION

Strata of the Transantarctic Basin (TAB) contain a complete South Polar sedimentary record of the global "icehouse" to "greenhouse" transition during the Early Permian (Collinson et al. 1994, 2006; Isbell et al. 2008b). Sedimentation in the TAB was dominated by glaciogenic processes during the Asselian–Sakmarian (Isbell et al. 2008c). This interval was part of the Late Paleozoic Ice Age (LPIA, ~ 374–256 Ma) (Fielding et al. 2008c; Montañez and Poulsen 2013). Widespread glaciation across Gondwana characterized the LPIA, as did low pCO_2, high pO_2, generally low eustatic levels with large magnitude fluctuations, low solar luminosity, and increased $\delta^{18}O$ and $\delta^{13}C$ values relative to the rest of the Phanerozoic (Gastaldo et al. 1996; Raymond and Metz 2004; Montañez and Soreghan 2006; Fielding et al. 2008d; Rygel et al. 2008; Montañez and Poulsen 2013).

The currently favored hypothesis for LPIA glaciations is that multiple ice centers (ice sheets or ice caps) were distributed across Gondwana, and that these ice centers grew and shank asynchronously over the LPIA's ~ 80 Myr duration (Fielding et al. 2008c; Isbell et al. 2012; Montañez and Poulsen 2013; López-Gamundí et al. 2021; Rosa and Isbell 2021). The character, distribution, and resulting sedimentary records of these glaciers would have been driven by global, regional, and local climatic and geologic influences (Isbell et al. 2012; Montañez and Poulsen 2013; López-Gamundí et al. 2021). The potential for local and regional heterogeneity of LPIA glaciogenic strata is therefore extremely high. To work towards an understanding of LPIA glaciation that can be tied to

Published Online: Month 2021

global trends, these successions must be understood on a local level before they can be correlated to basinal, regional, or global patterns.

In this paper, we evaluate the sedimentology, stratigraphy, and flow directions of four glaciogenic (Pagoda Fm) successions in the Shackleton Glacier region of the TAB (Fig. 1B). The Pagoda Fm in the Shackleton Glacier region has not previously been described and analyzed at the level of detail reported in this study. The Shackleton Glacier region can offer a different perspective to better-studied areas of the TAB (e.g., the Beardmore Glacier region) because it was located in a basin marginal position on the non-cratonic (or, "Panthalassan proximal") side of the basin during the deposition of the Pagoda Fm (Fig. 1).

GEOLOGICAL SETTING

Asselian–Sakmarian glaciogenic strata of the Transantarctic Basin (TAB) occur in discontinuous outcrops along the margin of the East Antarctic Craton from Victoria Land, near Australia, to Dronning Maud Land, near southern Africa (Frakes et al. 1971; Collinson et al. 1994; Isbell et al. 2008c) (Fig. 2A). During the lower Cisuralian, the TAB was a narrow ($\sim$ 100–200km-wide), trough-shaped basin that formed parallel and proximal to the Gondwanide margin of the East Antarctica Craton, but inboard of the Panthalassic margin (Fig. 3B) (Collinson et al. 1994; Elliot 2013; Isbell 2015; Elliot et al. 2017). In the central Transantarctic Mountains and Victoria Land, glaciogenic strata occur in four sub-basins: the Ohio Range to the Scott Glacier (Horlick Sub-basin), the Amundsen Glacier to the Darwin Glacier area (Beardmore Sub-basin), south Victoria Land (SVL), and north Victoria Land (NVL) (Figs. 1B, 3) (Frakes et al. 1966; Isbell et al. 2008c; Isbell 2010; Cornamusini et al. 2017). The Shackleton Glacier region is located near the southern edge of the Beardmore Sub-basin.

The origin and nature of the TAB during the Lower Permian is not well understood. Hypotheses include intracratonic and extensional settings (Collinson et al. 1994; Isbell 2015; Elliot et al. 2017). Regardless of what processes drove basin formation at that time, the TAB was a narrow, trough-shaped basin, with Proterozoic and early Paleozoic basement shoulders, that paralleled the Panthalassan margin of the East Antarctic Craton during deposition of the Pagoda Fm (Fig. 3) (Isbell et al. 1997b). Though there is no evidence for upper Carboniferous to Sakmarian orogenic activity in the central Transantarctic Mountains or adjacent Marie Byrd Land, volcanic arcs and tectonic compression were occurring elsewhere along Gondwana's Panthalassan margin during that time, including in eastern Australia, the Andean margin of South America and Patagonia, the Ellsworth Mountains, Thurston Island, and the Antarctic Peninsula (Fielding et al. 2001; Elliot 2013; Vizán et al. 2017). This same margin was extremely active and subject to repeated, complex accretion events throughout the Paleozoic (Veevers et al. 1994; Domeier and Torsvik 2014; Goodge 2020). As a result of this activity, the TAB evolved into a foreland basin later in the Permian (Collinson et al. 1994; Elliot et al. 2017). During the Lower Jurassic, strata in the central Transantarctic Mountains were pervasively intruded by sills associated with Ferrar Group volcanism and the breakup of Gondwana (Elliot 1992).

SEDIMENTOLOGY AND STRATIGRAPHY OF THE PAGODA FORMATION

The Pagoda Fm is the basal unit in the Permian–Early Jurassic Victoria Group (upper Beacon Supergroup) in the Beardmore Sub-basin of the TAB. Rare palynomorphs and conchostracans suggest that the Pagoda and Mackellar fms are Asselian–Sakmarian (Masood et al. 1994; Askin 1998; Babcock et al. 2002). The Pagoda Fm overlies both the Kukri and Maya regional erosional surfaces (Figs. 1B, 3) (Collinson et al. 1994; Isbell 1999; Elliot 2013). The Maya Erosional Surface is a disconformity that separates Devonian(?) clastics of the lower Beacon Supergroup from the Victoria Group (Isbell 1999). The Kukri Erosional Surface separates the Beacon Supergroup from underlying Ross Orogeny intrusions and associated metasediments. Significant relief of at least 150 m occurs on these unconformities (Fig. 4) (Isbell et al. 1997a, 2008c; Isbell 1999). Both the Pagoda Fm, and the overlying, post-glacial Mackellar Fm, lap onto the erosional surfaces, indicating that the Pagoda Fm and its equivalents in other sub-basins often did not overtop the relief (Isbell et al. 1997a). The lower Beacon Supergroup units are not present in the Shackleton Glacier region, and the erosional surface underlying the Pagoda Fm is merged Maya and Kukri surface (Isbell et al. 2008c). At all sites in this study, the Pagoda Fm overlies Ross Orogeny granites.

Since their discovery, the Pagoda Fm and its equivalents throughout the Transantarctic Mountains have been unanimously interpreted as glaciogenic or glacially influenced because their predominant lithologies are massive and laminated, sandy and silty diamictites (Long 1964a; Lindsay 1970a; Coates 1985; Barrett et al. 1986; Collinson et al. 1994; Isbell et al. 2008c). Minor lithologies of the Pagoda Fm include conglomeratic sandstones, sandstones, mudrocks, and lonestone-bearing mudrocks (Isbell et al. 2008c). Besides diamictites and lonestones, evidence for a glacial origin for the Pagoda Fm includes striated and polished basement surfaces, the prevalence of striated and faceted clasts, and a clear relationship between local basement composition and lithologies of large clasts in the diamictites (Lindsay 1969; Coates 1985). Detailed interpretations of depositional environments have been made for a few Pagoda Fm localities (Lindsay 1970a; Waugh 1988; Miller 1989; Isbell et al. 2001; Lenaker 2002; Long et al. 2008–2009; Koch 2010; Koch and Isbell 2013) and its equivalents in Victoria Land (Askin et al. 1971; Barrett 1972; Barrett and McKelvey 1981; Isbell 2010; Cornamusini et al. 2017), Horlick Mountains (Frakes et al. 1966; Aitchison et al. 1988), and Ellsworth Mountains (Ojakangas and Matsch 1981; Matsch and Ojakangas 1991). With few exceptions, these analyses have invoked subaqueous, glacial-proximal depositional settings. This is in contrast to early surveys that interpreted diamictites as subglacially deposited "tillites" (Lindsay 1970a; Coates 1985; Miller 1989; Isbell et al. 1997b).

Isbell et al. (2008c) separated the Permian glaciogenic units in the Transantarctic Mountains into basin-margin and basinal facies associations. Basin-margin successions are predicted to occur near basement highs and along basin margins, are relatively thin ($<$ 100 m), contain evidence for subglacial deformation and erosion, have deformation resulting from proglacial glaciotectonism, and small (m-scale) gravity-driven deposition. Basinal successions are thicker (100–500 m), have little-to-no evidence for subglacial processes, and are more likely to contain stratified diamictites, lonestone-bearing mudrocks, mudrocks, and larger (up to tens of meters) mass-transport deposits. Evidence of grounded ice and grounding-line processes have been identified in both basinal (e.g., Koch and Isbell (2013)) and basin-margin (e.g., Isbell (2010)) facies associations. Based on its paleogeographic position and Pagoda Fm thickness, the Shackleton Glacier area is here predicted to contain the basin-margin facies.

In the Shackleton Glacier region, the glaciogenic facies of the Pagoda Fm are underlain by a non-glacial, lacustrine facies association at a single site on Mt. Butters (site MB-17). This facies and its depositional environment are described in detail by Isbell et al. (2001). Below this contact, the fine-grained lacustrine facies are pervasively sheared, likely subglacially (Isbell et al. 2001). Lonestones, interpreted to be iceberg-rafted debris, occur in the lower post-glacial Mackellar Fm in the Shackleton Glacier region (Seegers 1996; Seegers-Szablewski and Isbell 1998). This suggests that glaciers were still present in the Transantarctic Basin even after glaciogenic sedimentation was no longer dominant.

STUDY AREA AND METHODS

The sedimentary sections described in this paper were examined as part of the U.S. Antarctic Program's helicopter-supported Shackleton Glacier Deep-Field Camp during the 2017–2018 austral summer (Table 1; Fig.

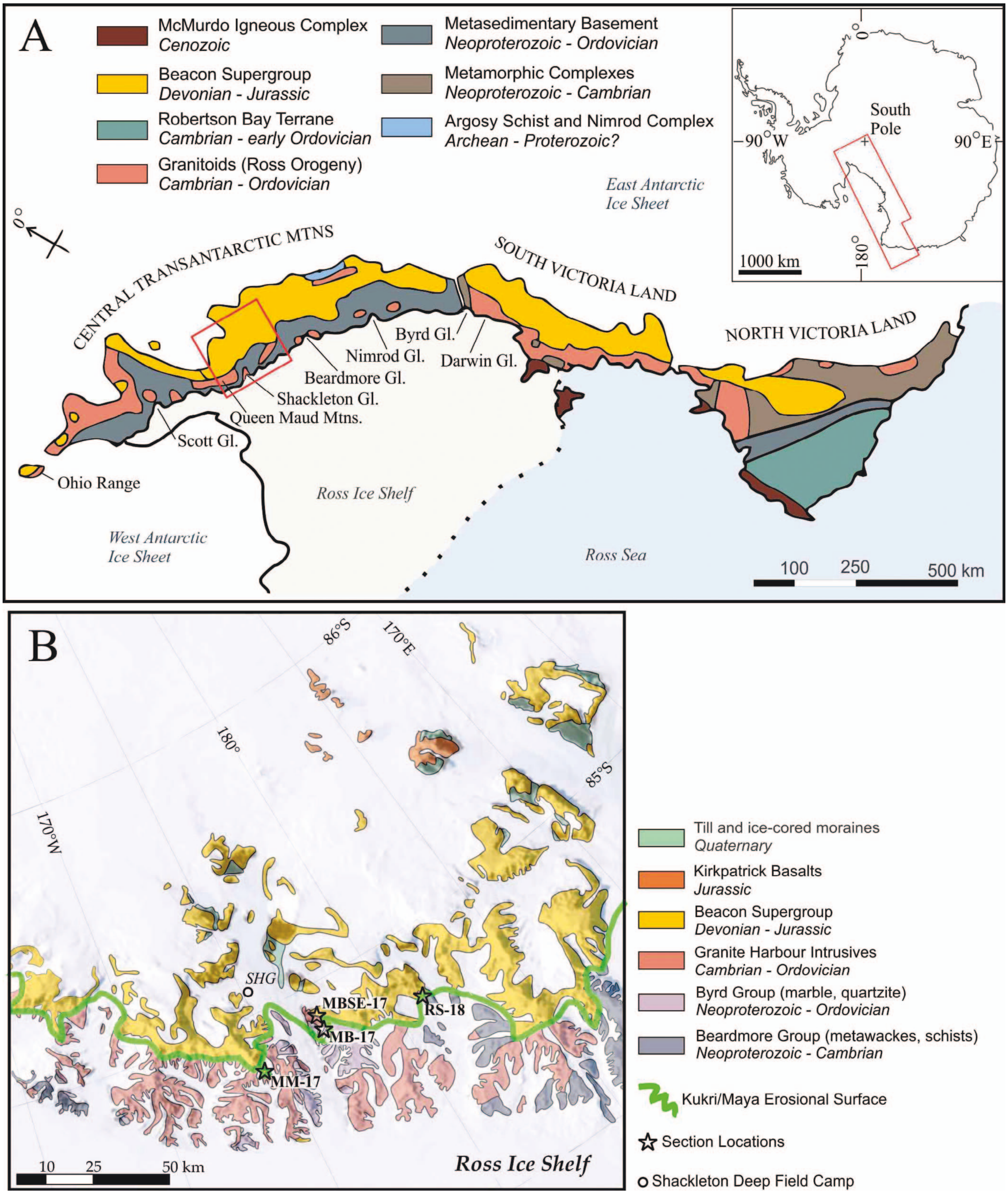

FIG. 1.—Generalized geologic maps of study area. Maps are South Polar projections. **A)** Geologic map of the Central Transantarctic Mountains and Victoria Land, with relevant outlet glaciers and mountain ranges labeled. Modified after Elliot (2013), Goodge and Fanning (2016), and Estrada et al. (2016). Box on inset map indicates extent of this geologic map. Red box on geologic map indicates the extent of "map B." **B)** Regional geologic map of the Shackleton Glacier area, noting the locations of sections described in this study. MM-17 is Mt. Munson, MB-17 is Mt. Butters 1, MBSE-17 is Mt. Butters 2, and RS-18 is Reid Spur. Geology adapted from McGregor and Wade (1969), and Mirsky (1969), aerial photos from LIMA Landsat imagery (Bindschadler et al. 2008).

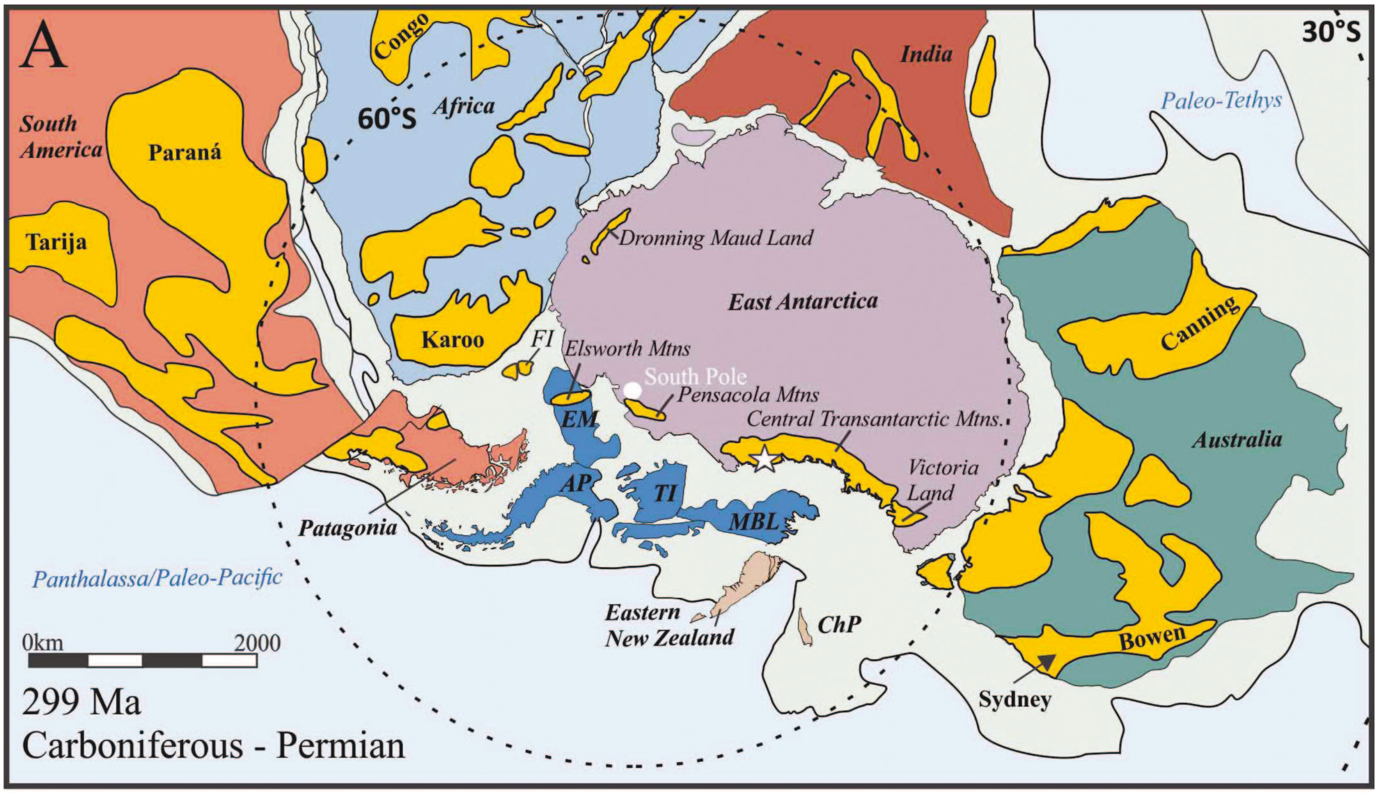

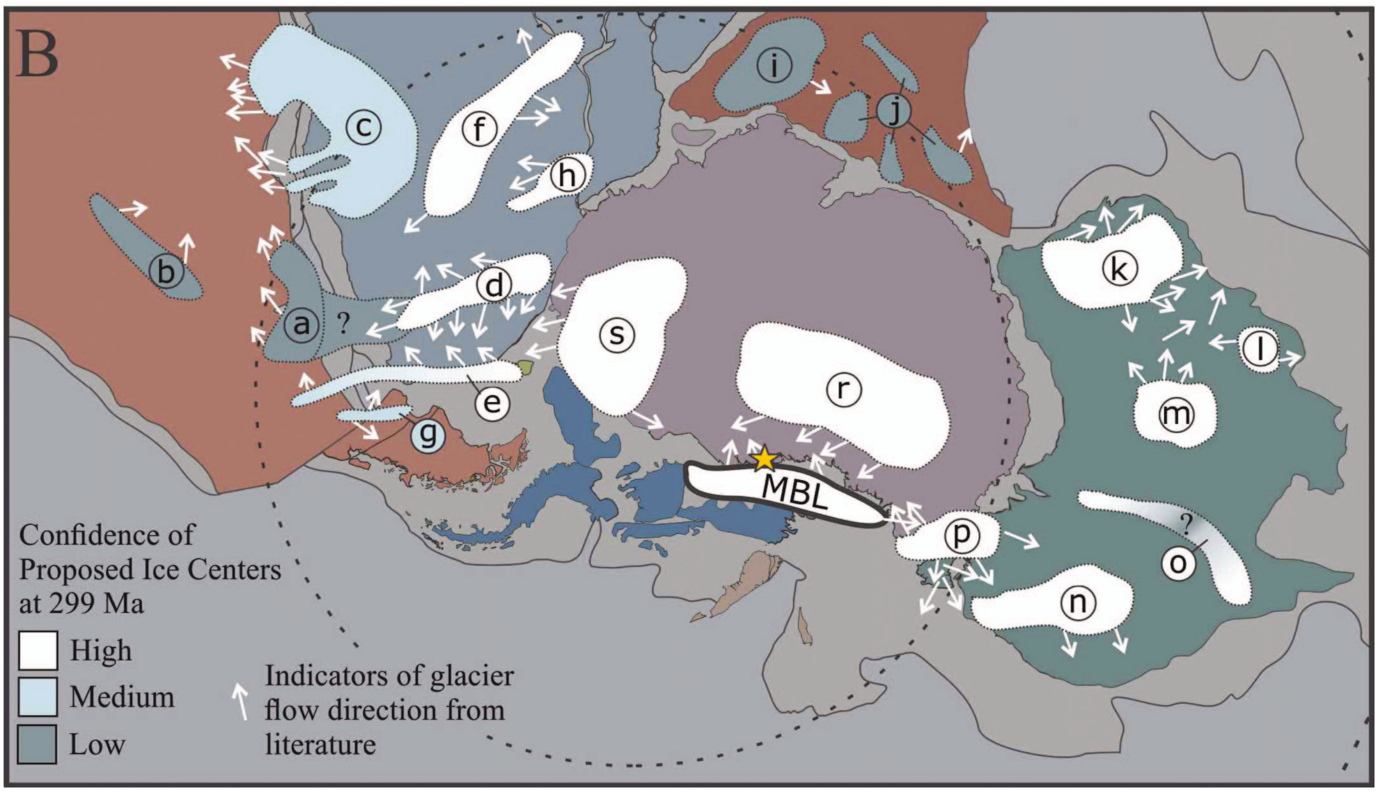

FIG. 2.—Paleogeographic reconstructions of Gondwana near the Carboniferous–Permian Boundary. All maps are south-polar projections. Star indicates the approximate location of the Shackleton Glacier area. Continent distributions and paleolatitudes are based on Lawver et al. (2011) and copied from Isbell et al. 2012). Note that there are differences in the positioning of some crustal blocks (e.g., Patagonia and New Zealand) between this reconstruction and Figure 3, which is modified after Elliot (2013). **A)** Yellow regions indicate the modern extent of sedimentary basins containing Late Paleozoic Ice Age strata. Abbreviations include: Falkland Islands–Malvinas (FI), Ellsworth Mountain block (EM), Antarctic Peninsula (AP), Thurston Island (TI), Marie Byrd Land (MBL), and the Challenger Plateau–western New Zealand (ChP). Basins are adapted

TABLE 1.—*Names and locations of sedimentary sections described in this paper.*

Location Name	Section Name	Geographic Coordinates	Thickness of Pagoda Fm
Mt. Butters 1	MB-17	S84° 51.029′ W177° 25.216′	90 m
Mt. Butters 2	MBSE-17	S84° 53.003′ W177° 22.354′	77 m
Reid Spur	RS-18	S84° 47.035′ E178° 46.680′	> 62 m
Mt. Munson	MM-17	S84° 45.359′ E173° 41.118′	5 m

1B). These sections are located on the Mt. Butters Massif (MB-17, MBSE-17) on the west side of the Shackleton Glacier, on the east face of Reid Spur (RS-18) of the Ramsey Glacier, and Mount Munson (MM-17) at the head of Barrett Glacier. The two sections at Mt. Butters are separated by approximately 2 km.

Sites were selected for section descriptions based on accessibility, continuity of exposure, and preliminary observations from previous expeditions to the area. At MB-17 several shorter sections were measured to capture lateral variability. Sedimentological data (texture, grain shape, sedimentary structures, etc.) as well as paleotransport indicators (including cross stratification, primary current lineations, striae, slickenslides, fold hinge lines, and thrust-plane orientation) were logged in each section. Measured sections were placed in context using outcrop-scale photographs taken from helicopters (Fig. 4).

Structural and sedimentary orientations were measured using a Brunton compass, with the azimuth set to 000°. Measurements were corrected for magnetic declination using the NOAA Magnetic Declination Estimated Value Calculator (NOAA 2019). Orientations were corrected for structural dip and aggregate orientations calculated using Stereonet (v. 11) software (Allmendinger et al. 2012; Cardozo and Allmendinger 2013). Some measurements from Mt. Munson were collected by JLI during the 1997–1998 field campaign to the Shackleton Glacier region. New flow-direction measurements are in Table 2 and site descriptions are in Appendix A.

FACIES ASSOCIATIONS

The following descriptions are of glaciogenic facies associations (FA) that constitute the Pagoda Fm in the Shackleton Glacier region (Table 3). We use the term glaciogenic to refer to sedimentary systems whose components are dominantly derived from glacial erosion and/or transport, and whose depositional processes are glacier-driven. For example, a succession that is the result of a plume from a subglacial jet would be glaciogenic, but largely non-glacially-derived deep-water sediments with the occasional outsized clast would instead be considered "glacially influenced." The characteristics of distinct sediment grain sizes are consistent throughout these successions. Very-fine-grained sandstones and shales are black in color. Fine- to medium-grained sandstones are generally quartz-rich with some lithic and potassium feldspar grains. Cobble- and boulder-size clasts are sourced from local basement lithologies (Fig. 1B), and include predominantly phaneritic granitoids, with some gneiss, quartzite, and gray, fine-grained metasedimentary rocks. All sand-size and coarser-grained material in the Pagoda Fm occurs in all categories of particle roundness (angular to well rounded), although finer-grained sands are typically better-rounded than medium- and coarse-grained sands. Striations occur on large clasts throughout the Pagoda Fm but are not common. The lack of striations is possibly due to the hardness of individual clasts, which are primarily composed of granite, quartz, and feldspar (Dowdeswell et al. 1985; Bennett et al. 1997).

Massive Sandy Diamictite Facies Association (MSD)

MSD Description.—This diamictite is the dominant FA of the Pagoda Fm. Similar lithologies occur throughout the Transantarctic Basin. In the Shackleton Glacier region, the thickness of this FA ranges from 3 m at Mt. Munson (MM-17) to 73 m at Mt. Butters (MB-17C). Since this diamictite is almost wholly massive, there is no clear way to further subdivide these successions. Where exposed, the lower contact overlies either a striated and polished unconformity with the Queen Maud Batholith (MM-17 and MBSE-17) or subglacially deformed lacustrine sediments (Isbell et al. 2001; MB-17C). The upper contact of this FA is sharp or erosional with current-transported facies, including the Cross Bedded Sandstone (CBS) facies association, the Heterogenous Sandy (HS) facies association, and the Mackellar Fm. The contact between this FA and the HS facies association is also gradational where facies HS1 (stratified diamictite) is present above the contact. The upper part of this FA are intercalated with turbidites (see LS facies interpretation), and may interfinger with stratified diamictites and mass-transport deposits (see HS facies association interpretation).

Approximately 90% of this FA is clast-poor to clast-rich diamictite (Hambrey and Glasser 2003; Hambrey and Glasser 2012) with minor amounts of sorted sands and gravels (Fig. 5). Clast abundances fluctuate throughout the succession. Some intervals are sufficiently clast-poor that they could be classified as muddy sandstones with dispersed clasts (< 1% clasts) (Fig. 5F) (Moncreiff 1989; Hambrey 1994; Hambrey and Glasser 2012). Most clast-rich parts of this diamictite contain 10–15% clasts (Fig. 5A, E), but some very limited areas contain up to ~ 30% clasts (Fig. 5C). Clasts range from pebble-size to 4 m in diameter. Clast compositions includes granite, feldspar, vein quartz, gneiss, and fine-grained metasandstone. Clast shape ranges from rounded to angular. Faceted clasts are common, but bullet-shaped and striated clasts are rare. The matrix is very poorly sorted, with sizes ranging from muds through granule-size grains. Matrix grain-size distributions remain constant within and between outcrops of this facies, though mean matrix grain size increases slightly in clast-rich sections relative to clast-poor sections.

The diamictite in this FA is massive, with very rare exceptions. However, broadly defined zones of clast-poor or clast-rich diamictites do

←

from Isbell et al. (2012). **B)** Proposed positions of glacial centers during the Early Permian based on flow directions and position of basins and "highlands." Illustrated ice centers are not meant to represent the whole possible extent of each proposed glacier, but where proposed glaciers were likely to be nucleated. The arrows reflect field measurements of flow directions reported in the studies cited for each ice center. However, flow directions of glaciers are highly variable, both spatially and temporally, and the true flow paths of these ancient ice centers were likely much more variable than the arrows on this map. Confidence is based on abundance of available lithologic data, and both relative and absolute ages. Ice centers are as follows: MBL, The proposed Marie Byrd Land ice center, discussed in this study as the most likely source for the glaciogenic sediments of the Pagoda Fm in the Shackleton Glacier region (Isbell et al. 1997b; Isbell 2010), a) Uruguay (Crowell and Frakes 1975; Assine et al. 2018; Fedorchuk et al. 2019), b) Asunción (Frakes and Crowell 1969; França and Potter 1988; Limarino et al. 2014), c) Windhoek–Kaokoveld Highlands (Martin 1981; Visser 1987; França et al. 1996; Rosa et al. 2016; Tedesco et al. 2016; Assine et al. 2018; Dietrich et al. 2019; Fallgatter and Paim 2019), d) Cargonian Highlands (Crowell and Frakes 1972; Visser 1997; Isbell et al. 2008a; Dietrich et al. 2019), e) Cape–Ventana Fold Belt (Visser 1997; Isbell et al. 2008a; Wopfner 2012), f) East African Thermal Rise (Rust 1975; Wopfner 2012), g) Patagonian Western Magmatic Arc (Pauls 2014; Survis 2015; Marcos et al. 2018), h) Zimbabwe (Wopfner 2012; Dietrich et al. 2019), i) Madagascar–SW India (Veevers and Tewari 1995; Isbell et al. 2012), j) Chotanagpur and Chhattisgarh (Veevers and Tewari 1995; Dasgupta 2006; Isbell et al. 2012), k) Pilabra–Yilgarn, l) Kimberly (see Mory et al. (2008); Martin et al. (2019), and references therein, m) Arunta–Musgrave (Mory et al. 2008 and Martinet al. 2019) and references therein, n) Bowen–Gunnedah–Sydney (Fielding et al. 2008a, 2008b, 2010), o) Galilee (Fielding et al. 2008a, 2008b, 2010; Isbell et al. 2012), p) Wilson (Hand 1993; Rocchi et al. 2011; Jordan et al. 2013), r) East Antarctic (Isbell et al. 1997a; Isbell 2010), s) Ellsworth (Frakes et al. 1971; Ojakangas and Matsch 1981; Matsch and Ojakangas 1992; Visser 1997).

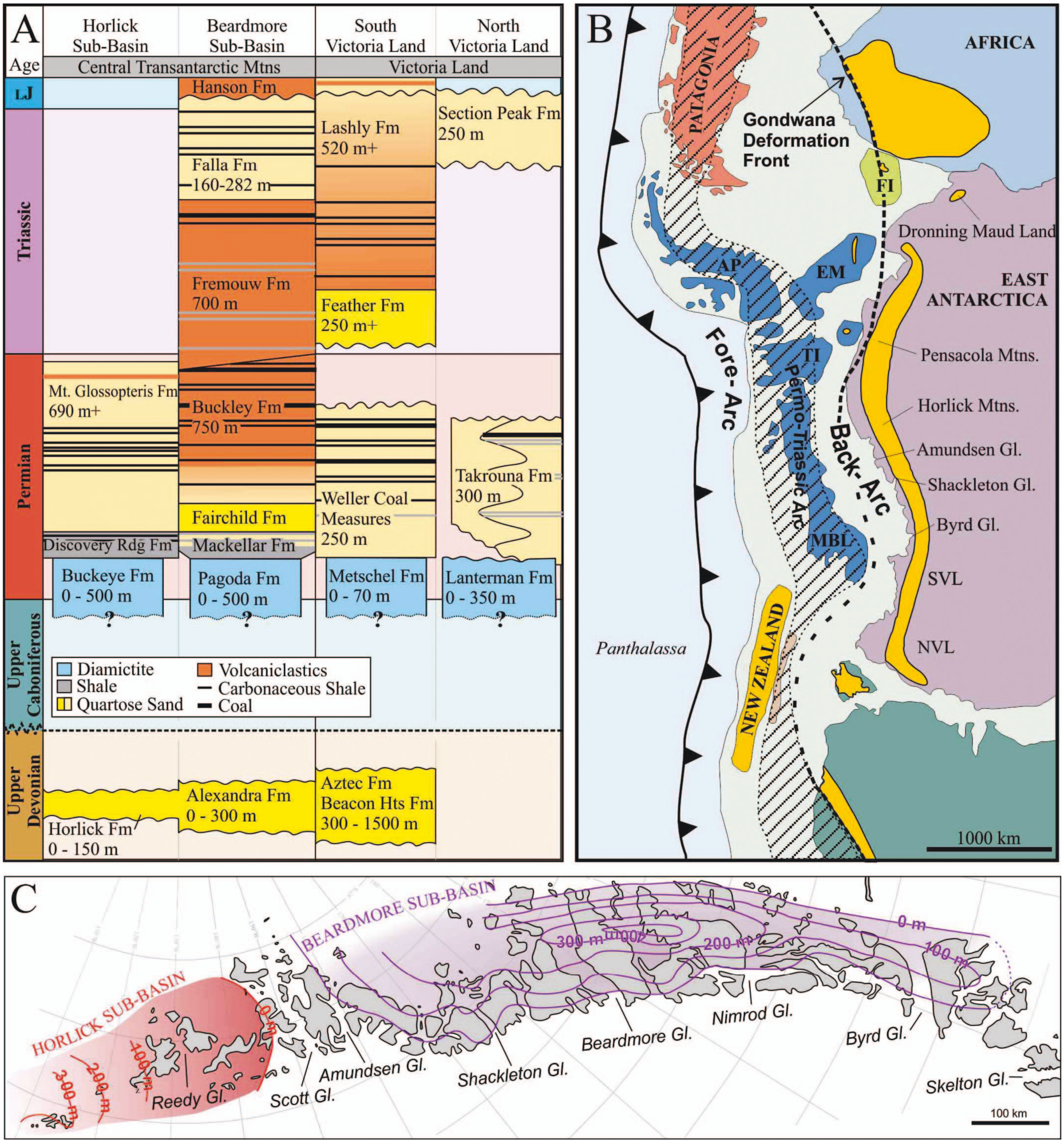

FIG. 3.—Regional geologic context and tectonic setting of the Transantarctic Basin during the Asselian–Sakmarian. **A)** Stratigraphy of the Beacon Supergroup across different regions of the Transantarctic Basin. Adapted from Elliot (2013), Cornamusini et al. (2017), and Elliot et al. (2017). **B)** Tectonic setting of southern Gondwana during the Permian, adapted from Elliot (2013). Regions of sedimentary deposition are shaded yellow. Note that there are differences in the positioning of some crustal blocks (e.g., Patagonia and New Zealand) between this reconstruction and Figure 2. **C)** Modern extent and isopach map of the Asselian–Sakmarian glaciogenic facies (Pagoda Fm and equivalents) in the Horlick Sub-basin and Beardmore Sub-basin in the Transantarctic Mountains. Gray areas are outcrops (nunatuks). Lines show isopachs of the Pagoda Fm (Beardmore Sub-basin) and Buckeye Fm (Horlick Sub-basin) from Isbell et al. (2008c).

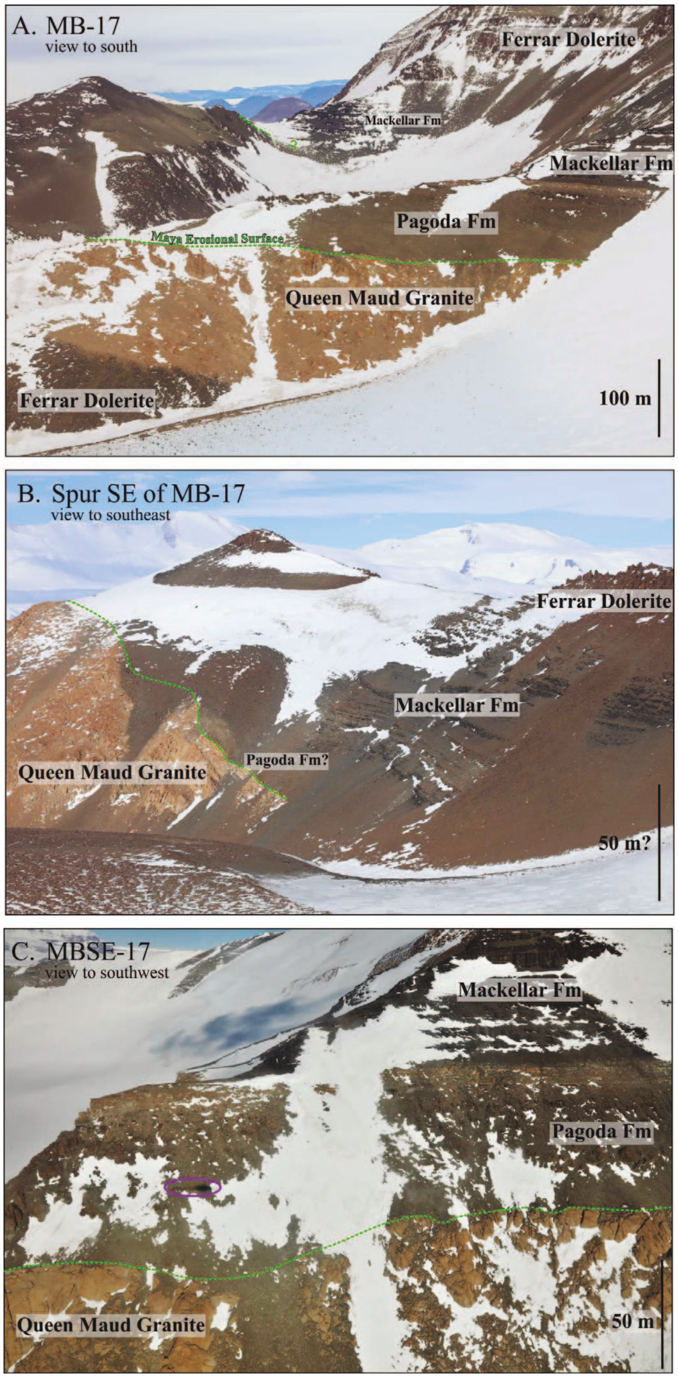

FIG. 4.—Photographs of Mt. Butters outcrops showing the stratigraphy of the Pagoda Fm and postglacial Mackellar Fm, and well as the relief of the Maya Erosional Surface, in this area. Formations are labelled, and the Maya Erosional Surface is marked by a green, dashed line. **A)** A photograph of section MB-17 taken from a helicopter; view to the south. The saddle in the background of this photo is approximately halfway between section MB-17 and MBSE-17. **B)** An outcrop that is part of the Mt. Butters Massif, and occurs on a spur located southeast of section MB-17. View is toward the southeast from MB-17. This site has never been visited on foot, so the scale is not certain. Note the dip of the granitic basement towards the southwest, which is consistent with basement dip measurements at site MB-17 and MBSE-17 in this study. This exposure is the same as Figure 4 in (Isbell et al. 2001). **C)** Photograph of section MBSE-17, view toward the SW. Purple oval shows helicopter's shadow.

occur. These zones are anywhere from 1 to 30 m thick. While we tracked these changes in clast abundance vertically through the measured sections, it was not our impression that these "zones" have any sort of horizontal organization as might be implied by the terms "layers" or "horizons," and that there are no distinct bounding surfaces between these zones. The transitions between these zones are gradational. These gradational transitions occur on the decimeter to meter scale. There was no clear relationship between transition thickness and any other property of these rocks. Zones of diamictites with similar clast concentrations cannot be correlated between outcrops; the distribution of clast-poor and clast-rich diamictites appears to be unique to each locality.

Crude and chaotic bedding occur very occasionally in the otherwise massive diamictite. Where bedding can be discerned, the beds are 2–10 cm thick, laterally discontinuous, and internally massive. Rare sedimentary structures include ruck structures beneath large clasts (Fig. 5D) and thinning of beds over large clasts (Fig. 5H). Rare beds of boulders and cobbles occur in the lower part of this facies at both Mt. Butters sites (Fig. 5G). In all "boulder beds" the clasts were not striated, polished, or uniformly oriented.

Sandstone and/or conglomerate bodies are also rare within this FA. These bodies occur in the diamictite and are poorly to moderately sorted. The grain compositions in these bodies are similar to sand- to gravel-size grains in the diamictite. Most sand bodies are massive but can contain layers of discrete grains sizes. However, these layers are often highly deformed. Bodies of sorted sand and/or gravel occur in two distinct sizes. Small bodies consist of sorted sediments that most often occur as irregularly shaped, horizontally elongate lenses, "whisps," and boudinage-like bodies that are up to 20 cm thick and 100 cm long (Figs. 5A, B, E, F). Such structures may occur alone or, more frequently, in bands and zones up to 1 m thick. Occasionally, diapir-like structures made of sand and/or gravel, 1 to 2 m thick, are also present. These structures project upward into the diamict but are not associated with other sand or gravel bodies. Larger bodies of well-sorted sand or gravel range in thickness from 1 to 3 m and are laterally discontinuous. These bodies have the same grain-size distributions as the smaller bodies. Large sand bodies are typically massive, but where stratification does exist in the sands and/or gravels the beds are largely deformed and display water-escape structures. The large sand bodies thin laterally and have overturned folds on their thicker ends. In one instance, the main sand body was accompanied by smaller sand bodies that trailed off away from its thick end (comet-like structure) (Fig. 5F; Sandstone with dispersed clasts). The lower contact between the comet-like bodies and the surrounding diamictite has a slope of 30° to 35° above horizontal, and the underlying diamictite sometimes has a fissile structure, indicating shearing. Occasionally such contacts overlie smaller sand lenses, sheath folds, "whisps," and boudins.

MSD Interpretation.—This FA is most likely glaciogenic or glacially influenced. Evidence for glacial transport of sediment in this FA includes striations and polish on basement granites where diamictites rest directly on granite (MBSE-17 and MM-17), the very poor sorting of sediment in the system, and the presence of angular to rounded grains of all sizes, faceted and striated clasts, and large boulders composed of local basement lithologies. In glacial settings, massive diamictites, like the facies described here, may be the result of subglacial till deposition (Evans et al. 2006), settling from suspension of a meltwater plume (Visser 1994), settling from suspension and rain-out from icebergs and iceberg scouring (Dowdeswell et al. 1994; Lisitzin 2002), mass-transport deposits (Rodrigues et al. 2019), or debris flows (Powell and Molnia 1989). Glacial depositional environments that include these processes are subglacial, proglacial proximal (but outside the influence of the grounding zone), and grounding-zone-environments including ground-zone wedges (Batchelor and Dowdeswell 2015; Demet et al. 2019; Dietrich and Hoffmann 2019), morainal banks (Eidam et al. 2020), and ice-contact fans (Powell 1990;

TABLE 2.—*Summary of paleo-transport measurements from this study (mean is Fisher mean ± a99). Note that due to the proximity of the study locations to the south pole that the orientation of compass directions are not the same across the basin. Mack, Mackellar Fm; L. Pag, lower Pagoda lacustrine facies (Isbell et al. 2001); T, trend; P, plunge; D, dip angle; DD, dip direction; S, strike; *, measured during 1997 field season.*

Section (Height)	Facies/Fm	Feature	Measurement	Orientation	N
Site MW-18					
10 m above basement	Mack	Asymmetrical ripples	Transport	T: 322°, 312°, 002°	3
Site MM-17					
0 m	-	Striae on basement	Lineation	T: 180°	1
*0 m	-	Striae on basement	Lineation	T: 095° ± 3.7°	8
*4 m above base of Mackellar	Mack	Asymmetrical ripples	Transport	T: 157° ± 28.5°	7
13–17.5 m	Mack	Highly deformed slump features	Vergence	T: 109°, 104°, 114°	3
*4–48 m of Mackellar Fm	Mack	Asymmetrical ripples	Transport	T: 109° ± 20.0°	10
Site MB-17					
0 m	-	Dip and dip direction of basement	Mean pole to plane	T: 262° P: 79° ± 12	5
			Plane from mean pole	S: 352° D: 11° **DD: 262°**	
MB-17A/B	L. Pag	Symmetrical ripple crest axes	Mean lineation	T: 346° ± 6.0 °	17
MB-17B	L. Pag	Slickenside lineation	Mean	T: 006 °	1
MB-17C (12 m)	MSD	Fold axes and small thrust faults	Mean Vergence	T: 220°± 31°	7
MB-17C (20 m)	MSD	Plane of thrust faults	Vergence	T: 256°, 251°	2
MB-17C (58 m)	MSD	Slide surface	Planes	DD: 243°, 191° D: 15°, 35°	2
			Plane from mean pole	S: 117° D: 23° DD: 206 °	
MB-17C/D (73–81m)	HA	Asymmetrical ripples	Mean transport Spread	T: 325° 236° - 055°	30
MB-17C/D	HA	Cross beds	Transport	T: 346°, 356°, 356° 226°, 221°	5
MB-17D	HA	Climbing Ripples	Transport	T: 221°, 256°	2
MB-17C (84 m)	HA	Grooves (iceberg keel marks?)	Direction of shallowing	T: 253° ± 24 °	5
MB-17C (18 m above Pagoda)	Mack	Asymmetrical ripples	Mean Transport	T: 219° ± 39 °	7
Site MBSE-17					
0 m	-	Striae on Basement	Lineation	T: 311°, 316°	2
MBSE-17 (29 m)	MSD	Sheath fold hinge	Orientation Vergence	T: 016°, P: 20 ° 286 °??	1
MBSE-17 (31–32 m)	MSD	Thrust faults	Mean pole to plane	T: 263° P: 69°	7
			Plane from mean pole	S: 353° D: 21° DD: 083°	
			Vergence:	T: 263°	
MBSE-17 (54 m)	HA	Crenulations on slide sufrace	Lineation	T: 241°, 251°	2
MBSE-17 (61–68 m)	CBS	Cross beds and asymm. ripples	Mean transport	T: 208°± 29 °	7
MBSE-17 (21–26 m above Pagoda)	Mack	Asymmetrical ripples	Mean transport	T: 298°± 6 °	23
Site RSP-18					
24–48 m	LS	Cross beds, asymm. ripples, and PCL	Mean transport	T: 176°± 29 °	18
68–70 m	Mack	Asymmetrical ripples	Transport	T: 261°, 241°, 211° 281°	4

Benn 1996). The most likely depositional processes and environments for the MSD facies can be inferred by considering the unique features of this facies.

The subglacial deposition of this FA is not likely to have been the dominant process, but cannot be wholly ruled out. A tillite interpretation for the MSD FA is supported by the massive, poorly sorted nature of the diamictites. However, there is no strong evidence for glacier grounding (for example, striated pavements or continuous erosional surfaces) above the base of this facies. The boulder and cobble beds in this FA do not contain uniform oriented, bulleted, or striated clasts. This suggests that the boulder beds are lags; that they formed due to winnowing (Eyles 1988), not subglacial processes.

This FA was more likely deposited subaqueously than subaerially. In most of the sections measured in this study, the upper contact of the diamictite is conformable with, and in some cases, gradationally transitions into, various subaqueous facies (HS facies association). At section RSP-18, the massive diamictite is interstratified with turbidites, a subaqueous process (see LS facies interpretation). Additionally, there are no

TABLE 3.—*Description of facies and facies associations.*

Facies Association	Facies Name	Thickness	Lithology	Structures	Formative Process	Depositional Environment
Massive Sandy Diamictite (MSD)	–	5–75 m (at least)	Clast-poor to clast-rich, sandy diamictite; muddy sand matrix; minor amounts of discontinuous sand and gravel bodies	Diamictites are massive to crudely bedded and ungraded, sands are generally massive, and sometime laminated, but always highly deformed	Glaciogenic, subaqueous processes; likely a combination of mass transport, iceberg rainout, iceberg scouring, plume sedimentation, and subglacial till deposition	Glacier-proximal to glacier-intermediate, continental shelf
Laminated Sands (LS)	–	~ 17 m	Coarse to fine-grained, well-sorted sandstones; quartz-rich; subangular to rounded	Fine- to medium-grained sands that occur in thin, planar beds with primary current lineations; coarse-grained sandstones are trough cross-bedded; fine- to very-fine-grain sandstones are laminated, or thin-bedded with unidirectional ripples	High-density turbidites and/or a transitional concentrated density flow (Mulder and Alexander 2001)	Distal or medial portion of an ice-contact fan or delta
Heterogenous Sandy (HS)	**HS1:** Bedded diamictite	1–10 m	Clast-rich, sandy diamictite; matrix is moderately well-sorted	3–7 cm beds that are massive with sharp, planar, and laterally discontinuous contacts; soft sediment deformation associated with facies HA2	Glaciogenic, subaqueous processes; likely a combination of iceberg-rain-out and plume sedimentation	Subaqueous glacier-proximal and grounding-line fan system
	HS2: Chaotic sandstones	0–15 m	Conglomerates to very fine-grained sandstones	Bedding is usually massive, soft-sediment deformation is pervasive; few primary sedimentary structures preserved; secondary structures include fold noses, boudinage, faulting, shear structures above and below contacts, and ruck structures	Mass-transport, gravity-driven processes in the form of slides, slumps, and/or mass-transport deposits	
	HS3: Stratified sandstones	0–15 m	Coarse- to very fine-grained sandstones	Medium- to coarse-grained sandstones are thickly laminated to bedded with planar cross beds, trough cross beds, climbing ripples, 3D ripples that are asymmetrical or climbing, hummocky and swaly cross stratification, and symmetrical ripples with bundled upbuilding; very-fine and fine sandstones are laminated or thin-bedded include unidirectional ripples, some flaser ripples and climbing ripples; occasional, small-scale soft-sediment deformation occurs in all lithologies	Current- dominated transport and deposition, with some slumping; unconfined flow; poorly sorted sediment source; large variations in current velocities; occasional wave reworking	
—	**Cross-bedded Sandstone** (CBS)	10–30 m	Well-sorted, medium- to very coarse-grained quartz arenite sandstone; rare pebbles, cobbles, and conglomerates	Low-angle and trough crossbeds; crossbed sets range in thicknesses from ~ 15 cm to ~ 1.5 m; rare thin beds with asymmetrical ripples; occur within amalgamated channels in multi-storied, multi-lateral sand sheet $<$ 2 km wide	Strong tractive flow confined to a series of amalgamated channels; subaqueous	Unconfined, distributive flow; likely glacial-proximal subaqueous fan/ grounding-line fan

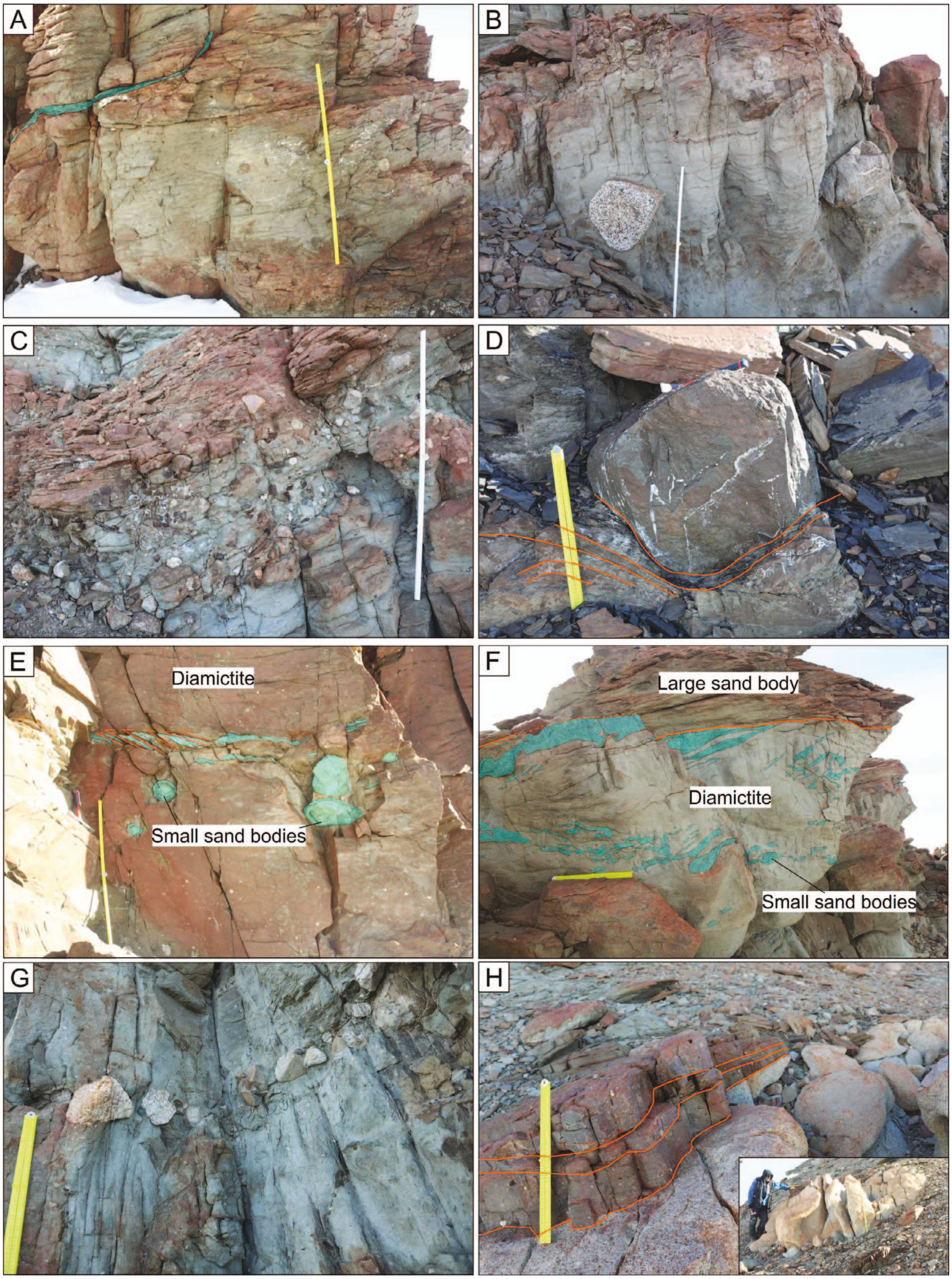

FIG. 5.—Photographs of the Massive Sandy Diamictite (MSD) facies association. Rulers are 50 cm long when folded in half and 1 m long when unfolded. Marks on rulers are in cm. The weathered color of the diamictite is gray to beige and tends to be redder when the matrix has a higher percentage of sand. Small sand bodies are highlighted by blue where present, and orange line indicates important bedding planes. **A)** A characteristic clast-poor section of the MSD facies association with a sand "whisp" (MB-17C). **B)** A diamictite section of this facies that is very clast poor, yet contains several large boulders (MB-17C). **C)** A clast-rich section of the MSD diamictite (MB-17C). **D)** A ruck structure in the diamictite made by a boulder (MM-17). **E)** Examples of small sand bodies in the MSD diamictite that experienced simple shear strain, resulting in sheath fold, "stringers," boudinage, and en echelon structures. (MBSE-17). **F)** Example of small sand-body bands in an otherwise massive, clast-poor diamictite. (MB-17C). **G)** A boulder and cobble bed in an otherwise massive diamictite (MBSE-17). **H)** Diamictite beds onlapping on to a large, 4 m boulder in the diamictite. Inset picture shows the whole, ∼ 4-m-diameter boulder in outcrop, with person for scale.

characteristics in this FA that suggest subaerial exposure (e.g., paleosols, desiccation features, wind-transported sediments).

The lack of clear or laterally continuous stratification, as well as a wide range of grain sizes in the matrix throughout this diamictite, indicate that the deposition of these sediments was not principally controlled by "sorting" processes such as currents and/or low-density flows. The massive nature of beds may be a primary depositional feature, as is the case in subglacial deposits, supraglacial debris, or subaqueous plume sedimentation. Alternatively, this facies may also be the result of secondary processes, such as redeposition by mass-transport and high-density gravity-driven processes–flows (Wright and Anderson 1982; Vesely et al. 2018), or homogenization due to iceberg scour (Dowdeswell et al. 1994), dewatering (Collinson and Mountney 2019), or bioturbation (Svendsen and Mangerud 1997; Murray et al. 2013). Where crude stratification does occur, there are indicators that settling from suspension may have been a key depositional process. Ruck structures beneath large clasts suggest those clasts were dropped into the surrounding diamictite from ice-rafted debris (Fig. 5D) (Thomas and Connell 1985). The thinning of diamictite beds over large clasts suggests that there was some component of settling from suspension in their depositional process (Fig. 5H). In glaciomarine settings, this most often occurs as meltwater plume sedimentation.

Small, deformed, sorted sediment bodies occur in many depositional settings alongside diamictites, including in till (Kessler et al. 2012) and proximal glaciomarine sediments (Domack 1983; Sheppard et al. 2000). Depending on their depositional context, small sand bodies are proposed to be sourced from iceberg dumps, winnowing due to dewatering, or from incorporating subglacial sediment into till through freeze-on. The small sand and gravel bodies all indicate pervasive simple shear (whisps, stringers, boudinage, and sheath folds) or loading (diapir structures). In at least one case, shearing was associated with an overlying, thicker sandstone body (Fig. 5F). If the diamictite experienced similar strain conditions, representative structures would likely be impossible to observe in outcrop, due to the homogeneous natures of the diamictite. The large sand bodies are most likely mass-transport deposits that underwent slumping or non-turbulent flow (Posamentier and Martinsen 2011; Rodrigues et al. 2019).

The combination of processes (subglacial till deposition, iceberg rain-out, plume sedimentation, iceberg scouring, and mass transport) that potentially contributed to the deposition of the massive diamictite and related facies are most likely to occur in a glacier-proximal to glacier-intermediate (not distal or proximal) setting, with water depths below storm wave base (i.e., offshore–transition to offshore) (Licht et al. 1999; Powell and Cooper 2002). In the Cenozoic, comparable depositional models have been proposed for similar successions in the Yakataga Fm, Alaska (Eyles and Lagoe 1990), Weddell Sea, Ross Sea, and George V regions of Antarctica (Anderson et al. 1980; McKay et al. 2009), as well as St. George's Bay, Newfoundland (Sheppard et al. 2000). Of these examples, St. George's Bay is likely the most analogous to the Shackleton Glacier region during the Permian, since it is not an open-shelf setting, but an embayment whose topography is controlled by much older basement rocks (Batterson and Sheppard 2000; Shaw 2016).

Plumes emitted from subglacial and englacial meltwater jets were likely the primary sources of sediments in this system. Plume sedimentation is not likely to occur where the glacier meltwater is denser than the ambient water in the depositional environment, which is a condition associated with lacustrine conditions and resulting hyperpycnal flows. Therefore the deposition of this facies most likely occurred in marine or estuarine conditions (Powell 1990). Variations in iceberg calving, fluctuating glacial hydraulic systems, and minor movement of the ice margin may explain the variation of matrix grain size and clast abundance throughout the facies. Glacial hydraulic systems and icebergs capable of producing sufficient sediment to create this FA are characteristic of temperate to "mild" subpolar glaciers (Matsch and Ojakangas 1991; Hambrey and Glasser 2012; Dowdeswell et al. 2016; Kurjanski et al. 2020).

The time frame in which the deposition of this facies occurred is difficult to infer, especially without any evidence in the facies for glacier grounding above its lower contact. Sedimentation rates in glaciomarine settings are highly variable, even for the same glacier, and strongly depend on glacier conditions and proximity to the ice front (Hallet et al. 1996). Rates of accumulation will also depend on physiography of the depositional area (e.g., fjord vs. open shelf). Accumulating $\sim$ 100 m of glaciomarine diamictite could take anywhere from a few years (Cowan and Powell 1991) to a few millennia (Partin and Sadler 2016; Domack and Powell 2018). The lack of non-glaciogenic deposits (see LS and HS facies descriptions for glacial interpretations) interstratified with the MSD facies suggests that the deposition of this facies occurred on the shorter end of this time scale.

Laminated Sands Facies Association (LS)

LS Description.—This is a sandstone FA that occurs only at site RS-18 and is interstratified with facies MSD. This succession is $\sim$ 17 m thick and laterally continuous across the outcrop. Its lower contact is erosional above MSD, and its upper contact was covered. Internally, this FA consists of fining-upward packages 3–5 m thick (Fig. 6). This FA consists of coarse- to fine-grained, well-sorted sandstones. The dominant lithology in this FA is fine- to medium-grained sands that occur in thin, planar-laminated beds with primary current lineations. Coarse-grained sandstones at the bases of some packages are trough cross-bedded. Fine- to very-fine grained sandstones are laminated, or thin-bedded with unidirectional cross-laminae and/or ripples. The sandstone is quartz-rich, and grains are subangular to rounded. Pebbles up to 8 cm in diameter occur at the bases of some cross-beds. The uppermost parts of fining-upward packages sometimes include fine- to very-fine-grained black-colored sandstone.

LS Interpretation.—This FA is most likely the result of a series of noncohesive density-flow events, in the form of high-density turbidites and/or a transitional concentrated density flows (Mulder and Alexander 2001). Fining sequences such as these could also be formed in a fluvial or shallow marine setting, where bedload-dominated currents are common. However, a fluvial setting is inconsistent with the lack of channelization or indication of surface exposure in the RSP-18 succession. Similarly, a shoreface setting is unlikely because there is no evidence of emergence or wave action in the succession. The current directions measured in this unit are unidirectional, which is also not indicative of a shoreface. Since these turbidites are interstratified with facies MSD, they are most likely the distal or medial part of an ice-contact fan or delta (Lønne 1995; Dowdeswell et al. 2015).

Heterogenous Sandy Facies Association (HS)

HS Stratigraphy

This FA (Fig. 7) occurs at both Mt. Butters sites above a gradational contact with the massive diamictite (MSD), and below a sharp, erosional contact with the cross-bedded sands facies (CBS) at MBSE-17 and a sharp, planar contact with the Mackellar Fm at MB-17 (Fig. 8). The lower part of the facies association begins as interbedded, discontinuous bodies of deformed, sorted sands and gravels (facies HS2) in stratified diamictites (facies HS1). Undeformed, moderately sorted, stratified sandstone bodies with a range of grain sizes (facies HS3) occur in the middle of the succession and eventually become the dominant facies near the top of the succession. This FA ranges in thickness from 1 to 15 m. Lithologies in this facies are interstratified.

FIG. 6.—Photograph of the Laminated Sands (LS) facies association at site RS-18 (Reid Spur). Triangles show fining-upward packages separated by erosional surfaces. Reddish lithologies are medium-grained sandstone to coarse-grained sandstone, and have planar lamination and low-angle cross-stratification. Black lithologies are fine-grained sandstones.

Facies HS1: Stratified diamictite

Description.—This facies is a clast-rich, sandy diamictite (Figs. 7D, G, I, 8). This diamictite facies is similar to the massive diamictite facies (MSD), but is consistently stratified, is more clast-rich, and the matrix is better sorted. The matrix in this facies is moderately to well sorted. Matrix grain sizes range from medium to very fine sand. The mean matrix grain size varies between beds. Most beds have a mean matrix grain size of medium sand, but some beds have a dominantly very fine grained sand matrix. Clasts in this facies are angular to subrounded, and have a size range similar to MSD, granule to 1 m boulders. The beds in this facies are 3–7 cm thick, are planar, laterally discontinuous, and have sharp contacts. The distribution of clasts is random and unrelated to bedding planes. Larger clasts often punctuate bedding planes. This facies has a gradational lower contact overlying the massive diamictite (MSD) facies. Vertical and lateral contacts with other facies in this FA (HS3 and HS2) are most often sharp, sometimes loaded, deformed, or erosional. This bedded diamictite is frequently interbedded with facies HS2. Strata in this facies adjacent to contacts with facies HS2 often display soft-sediment deformation, including load structures and sheared contacts.

Interpretation.—Similar to facies MSD, this facies was likely deposited in a glacier-proximal glaciomarine setting, but was dominated by plume sedimentation and iceberg rainout (Eyles 1987; Licht et al. 1999; Powell and Domack 2002; McKay et al. 2009). The consistency of the stratification in this facies compared to the MSD facies suggests that the sediment in this facies was not as frequently subject to remobilization, either through gravity-driven transport or iceberg scour. The better sorting of the matrix in this facies relative to the massive diamictite facies indicate that sediment-sorting processes were more active than during the deposition of MSD. In a glacial-proximal setting, this likely means that turbulence kept fine-grained sediment suspended in the water column and did not allow it to settle out. The clast-rich composition and the thin nature of the beds also suggest that depositional processes were relatively constant, compared to the high variability of clast contents in facies MSD. Loaded, deformed, and erosional contacts in this facies, and with other facies in this FA, indicate that this facies was rheologically "weak," or experienced ductile deformation at low strain magnitudes. Therefore, during and shortly following deposition, facies HS1 was likely water-saturated. This also suggests that that sedimentation was rapid, that this facies was subject to gravity-driven processes, and that these sediments were deformed by gravity-driven deposits (Figs. 7D, F, 8) (Visser 1994).

Facies HS2: Chaotic Sandstones

Description.—This facies consists of very fine- to coarse-grained sandstones (Fig. 7A–C). Beds in this facies are laterally discontinuous (Figs. 7G, 8). The thicknesses of sandstone bodies are laterally inconsistent and range in thickness from 0.5 m to 2 m. Widths of sandstone bodies range from ~ 1 m to outcrop scale. Sandstone beds may be interbedded with one another, but are dominantly interbedded with the surrounding either massive (MSD FA) of stratified (HS1) diamictite facies. Sandstone bodies are irregularly shaped, but generally have planar to lenticular shapes. Lower and lateral contacts are deformed, sharp, or erosional, and often show evidence of soft-sediment deformation (Fig. 7D, F). Upper contacts are sharp and conformable. Contacts between sandstone bodies are erosional or deformed.

Beds in this facies are often internally massive, and soft-sediment deformation is pervasive (Fig. 7E, F). Primary sedimentary structures are sometimes preserved, but this is rare and only occurs in a small area of any given bed. Secondary structures in this facies include fold noses (Fig. 7E), boudins, faults, and other simple shear structures above and below contacts (Fig. 7D–G), and ruck structures associated with rare outsized clasts (Fig. 7I). Grain size in this facies ranges from conglomerate to very-fine-grained sandstone. Fine- to medium-grained sandstones tend to be well sorted, while coarse-grained sandstones and conglomerates are poorly sorted. The medium- and coarse-grained sandstones occur more frequently than finer-grained lithologies.

Interpretation.—The sandstone bodies in this facies are most likely the result of mass-transport, gravity-driven processes (Posamentier and Martinsen 2011; Sobiesiak et al. 2018; Rodrigues et al. 2019). Preserved primary sediment structures in some of these bodies indicate that sediment sorting due to current transport likely occurred before the remobilization and final deposition of these sediments. Irregular lateral contacts between this facies and the two diamictites facies (HS1 and MSD) indicate that mass-transported bodies were sandstone rafts deposited into pre-existing diamictites by gravity driven processes. The deposition of mass-transport

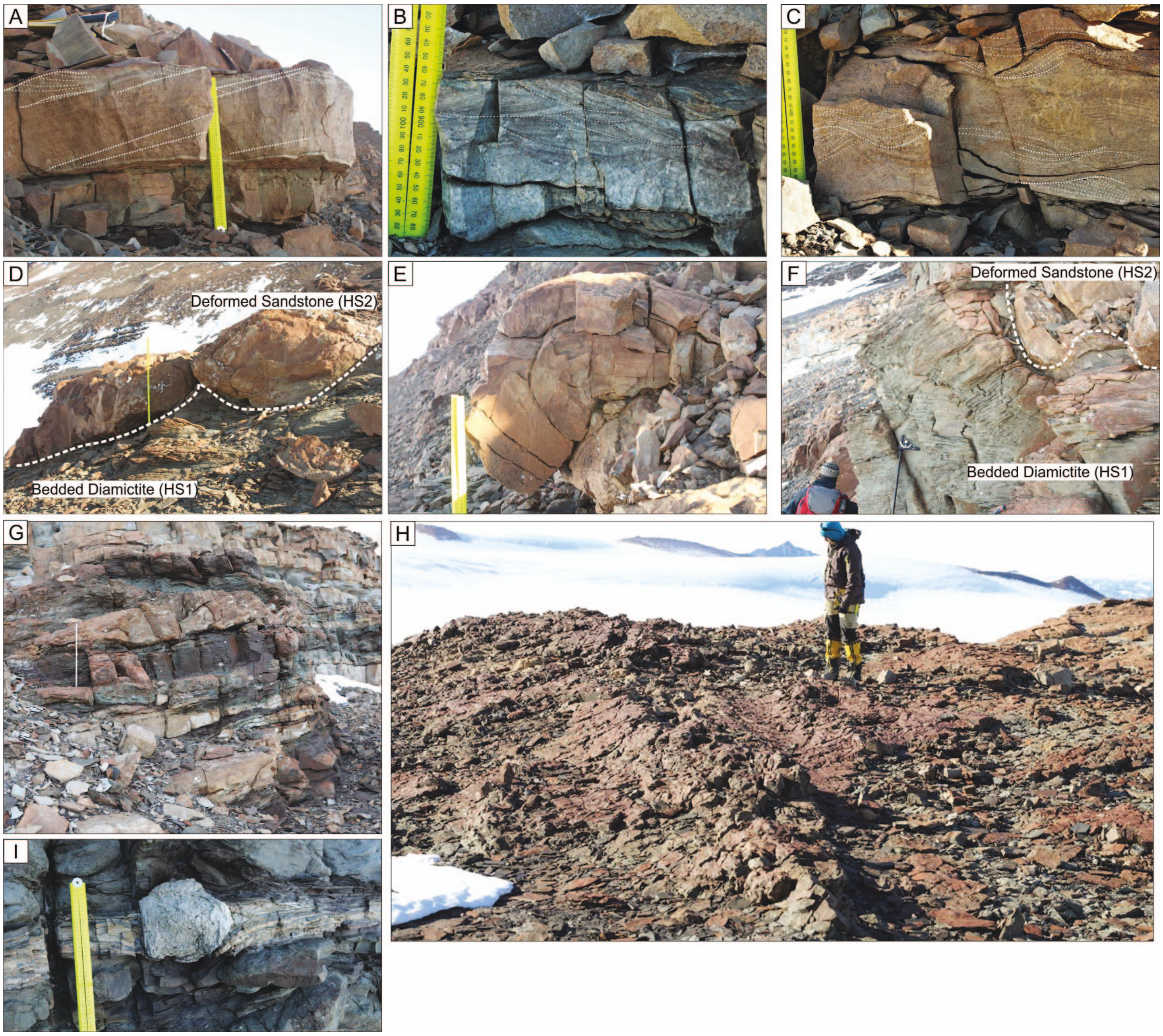

FIG. 7.—Photographs of the Heterogenous Sandy (HS) facies association at Mt. Butters in section MB-17 and MBSE-17. Marks on all rulers are in cm. Rulers are 50 cm when folded in half and 1 m long when unfolded. White dashed lines have been used to highlight contacts and important bedding surfaces. **A)** Medium-grained sandstone layer in facies HS3. The sandstone body is composed mostly of climbing dunes (cross beds) and capped by asymmetrical ripples. Note sharp contact with black-colored, bedded diamictite (facies HS1) in lower part of image (MB-17). **B)** Fine- to medium-grained sandstone in facies HS3 with up-building symmetrical ripples (MB-17). **C)** Swaly and hummocky cross-stratification in sandstone layer of facies HS3 (MB-17). **D)** Loaded, possibly boudinage, contact between a massive sandstone (HS2) and bedded diamictite (HS3) (MB-17). **E)** Sandstone with a soft-sediment recumbent fold nose in facies HS2, likely at the front of a slump (MB-17). **F)** Deformed contact between facies HS2 and HS3. Jacob's staff for scale; marking is every 10 cm. (MB-17). **G)** Outcrop showing interfingering between facies in this facies association. Black-colored sediments are bedded diamictites (facies HS1), other lithologies show sand and gravel of facies HS2. (MB-17). **H)** Groove structures on top of facies HS1. View approximately toward north (down the Shackleton Glacier). **I)** Granitic outsized clast punctuating interlaminated sandstone beds in the bedded diamictite facies HS1 (MB-17).

deposits (MTDs) into the diamictite indicates that diamictite deposition was contemporaneous with MTD emplacement. This also suggests that the diamictite was weak (highly susceptible to deformation), likely due to both high pore-water pressures and a lack of consolidation.

Facies HS3: Stratified Sandstones

Description.—This facies consists of these facies very fine- to coarse-grained sandstones (Fig. 7A–C). Medium- to coarse-grained sandstones are thickly laminated to bedded. Common sedimentary structures in medium- to coarse-grained sandstones include planar cross beds, trough cross beds, climbing ripples, and 3D ripples that are asymmetric or climbing (Fig. 7A). Rare sedimentary structures include hummocky and swaly cross stratification and symmetrical ripples with bundled upbuilding (Fig. 7B, C). Lateral and vertical variations in sedimentary structures within a unit of the same lithology or grain-size is common. Coarser sands are occasionally massive or contain laterally discontinuous sand or gravel lenses. Trough cross-beds occasionally have pebbles at the bases of

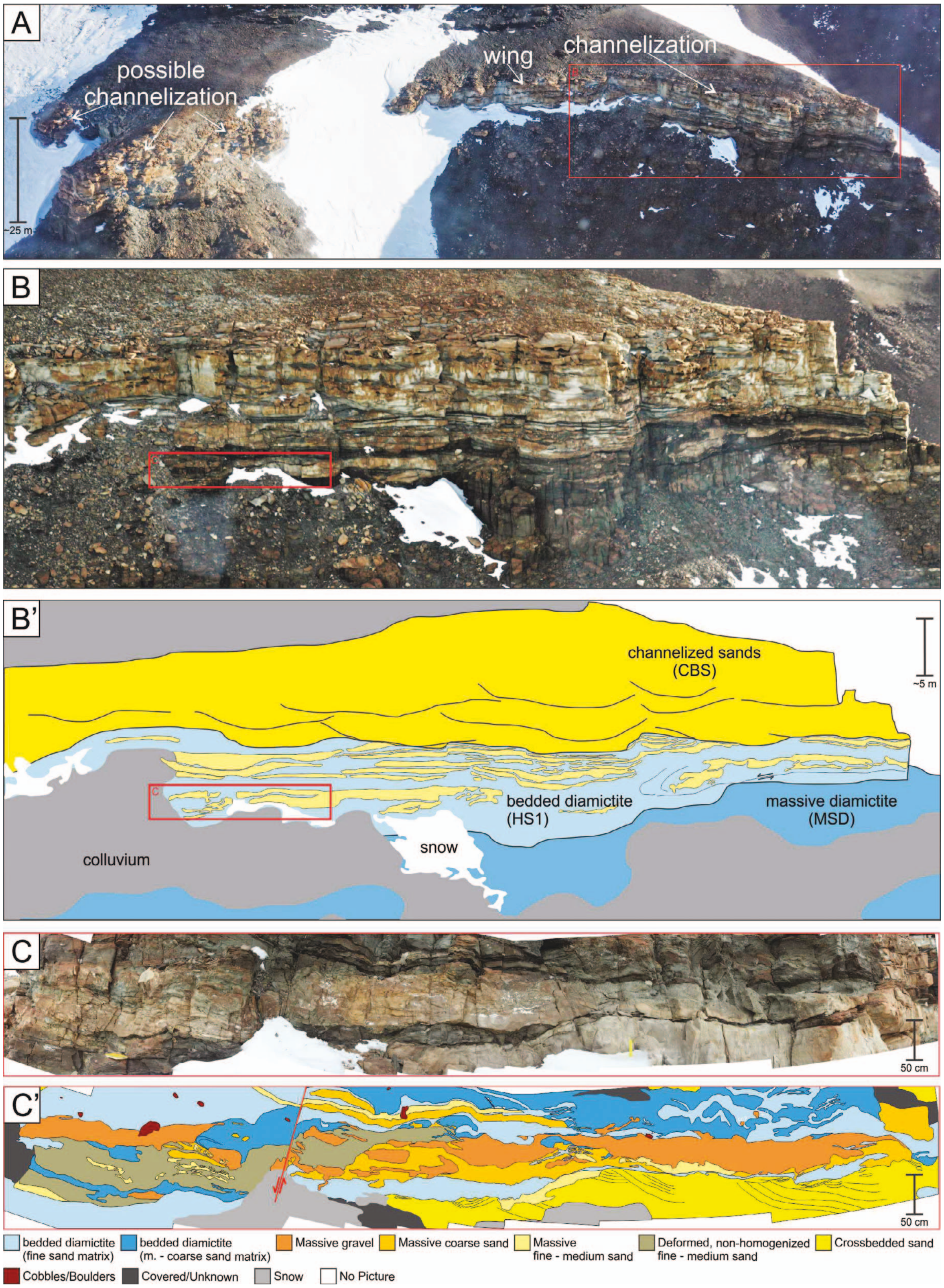

FIG. 8.—Photo mosaics (A, B, and C) and interpretive sketches (B′ and C′) of the upper part of section MBSE-17 at Mt. Butters. Mosaics A and B were taken from a helicopter, and mosaic C from the ground. This is the opposite side of the outcrop shown in Figure 4C. View is to the north, and the ridge runs roughly east–west. Part A shows lateral variations in the architecture of the cross-bedded sandstone (CBS) facies. Figures B and B′ highlight the stratigraphic relationships between the Massive Diamictite (MSD) facies association, the Heterogenous Sandy (HS) facies association, and the CBS facies association. Black lines in CBS denote channel erosional surfaces. Black lines in HS3 indicate soft-sediment deformation. The part of this outcrop highlighted by C and C′ is located within the red box on Part B. Part C shows a part of the outcrop that is characteristic of the HS facies association, and was selected to illustrate the pervasive nature of soft-sediment deformation in this facies association.

troughs. Very fine- and fine-grained sandstones are laminated or thin-bedded. Sedimentary structures in fine-grained and very fine-grained sandstones include unidirectional cross-laminae, ripples, planar and wavy laminae, some flaser-bedded cross-laminated units, climbing-ripple laminae, and rare outsized clasts with ruck structures. Lithologies of all grain sizes also have minor amounts of soft-sediment deformation, including dewatering structures, minor folds, and loading.

At the upper contact of the Heterogenous Sandy FA with the Mackellar Fm in section MB-17, these sandstones had at least five large, shallow, east–west-oriented grooves (Table 2) that occur in a massive, well-sorted sandstone (Fig. 7H). All grooves were $\sim$ 1–2 m wide and 10 cm deep. Berms $\sim$ 10–20 cm high bound the grooves on their long sides. All of the grooves gradually shallow towards the west (215°), and two of the grooves had prow-like berms at their eastern terminus.

Strata in this facies are laterally continuous across the outcrop. Sandstone bodies are generally wedge-shaped and thicken in the direction of flow. Erosional surfaces are common in the facies. This facies has an erosional lower contact with both diamictite facies (MSD and HS1), and a sharp, conformable contact with the overlying UFG facies association.

Interpretation.—This facies was likely deposited rapidly in an unconfined, subaqueous setting with limited reworking by waves and icebergs. The sedimentary structures in this facies indicate that current-dominated transport and deposition occurred, followed by syndepositional or postdepositional slumping of some deposits. The wide range of grain sizes and sedimentary structures indicate a sediment source with a wide range of grain sizes and huge variations in current velocities during deposition. Common sedimentary structures, such as planar cross beds, trough cross beds, and asymmetrical ripples, suggest unidirectional, relatively high-velocity currents. Climbing ripples suggest decrease in flow velocity downcurrent, which is characteristic of unconfined flows, which is supported by the lack of channelized deposits. Flaser bedding, as well as abrupt changes in grain size and sedimentary structures within and between beds, indicates that current velocities were highly variable and fluctuated. Rare soft-sediment deformation suggests high pore-water pressure during rapid deposition. Rare hummocky and swaly cross-stratification and symmetrical ripples form under oscillatory flow conditions created by surface waves, possibly during reworking by storms (Reineck and Singh 1980; Dumas and Arnott 2006; Collinson and Mountney 2019). Their rare occurrence and interstratification with fine-grained sediments suggest that these wave features formed below normal wave base. The shape of the grooves on the upper contact of this FA at site MB-17, their position in the upper contact of a massive (homogenized) sandstone, and immediately below the contact with the dropstone-bearing lower Mackellar Fm suggest that these features are iceberg keel marks (Dowdeswell et al. 1994; Vesely and Assine 2014). These massive sandstones were likely deposited in a similar way to other sandstones in this facies, but were homogenized by iceberg actions.

HS Depositional Environment.—The three facies in this FA represent a complex depositional environment that is characteristic of subaqueous, glacier-intermediate to -proximal settings in front of the terminus of temperate to "mild" subpolar glaciers. Evidence for the glaciogenic origin of this FA includes pebbles with ruck structures (representing ice-rafted debris), iceberg keel marks (facies HS3), the very poor sorting of sediment in the system, and the wide range of sedimentary grain shapes in the Pagoda Fm sandstones, which are described at the beginning of the facies section.

The stratified diamictite (facies HS1) was deposited primarily through plume sedimentation in a glacier-proximal setting, and is the dominant, or "background," sedimentation type in this FA. The gradational contact separating MSD (massive diamictite) and facies HS1 suggests a gradual shift in depositional environments between the two. Sediment composition is consistent between the two diamictite facies, suggesting that the sediment source did not change, but that the depositional environment shifted from glacier-intermediate to glacier-proximal. The deposition of both diamictites was likely controlled by the same processes (i.e., plume sedimentation, iceberg rain-out, iceberg scouring, and mass transport) but to different degrees. This shift from glacier-intermediate to glacier-proximal was most likely driven by a minor readvance of the glacier margin, but it may have also been an apparent effect caused by the progradation of the overlying grounding-line fan system (HS2 and HS3).

The sandstone facies in this FA (facies HS2 and HS3) most likely represent the medial part of a subaqueous grounding-line fan(s) system (Powell 1990; Lønne 1995; Dowdeswell et al. 2015). In facies HS3, the high-velocity, unidirectional current transport combined with abrupt changes in grain size (i.e. current velocity), unconfined flow, and interstratification with the bedded diamictite (facies HS1) are characteristic of grounding-line fans (Powell 1991). The gravity-driven transport of facies HS2 sandstone bodies were likely derived from deposits similar to (or the same as) facies HS3. "Shedding" of sediments is characteristic of the rapid sedimentation in grounding-line fan systems (Benn 1996; Powell and Alley 1997; Lønne et al. 2001). Intense, ductile deformation and loading along contacts throughout this FA indicate that all facies were water-saturated, unconsolidated, and generally had the consistency of soup, suggesting rapid deposition and that they were therefore prone to resedimentation (Fig. 8B).

The wave reworking of some sandstone beds, as indicated by hummocky and swaly cross-stratification and wave-ripple stratification (symmetrical ripples) in facies HS3 suggest that this depositional environment was occasionally subjected to surface-wave activity (below normal wave base). These features indicate that there was not perennial ice cover during the deposition of this FA. This evidence for wave reworking suggests a similar, wave-winnowing origin for the boulder beds in facies MSD.

Where this FA is well developed in outcrops at Mt. Butters (sites MB-17 and MBSE-17), the succession has a general coarsening and increase in sorting trends upward. This trend indicates the increase in the proximity of the energy and sediment source, either through progradation of the grounding-line system and/or advance of the glacial front.

Cross Bedded Sandstone Facies (CBS)

CBS Description.—This facies occurs at Mt. Butters section MBSE-17, and consists of an erosionally-based, laterally extensive, channel-form sandstone body 10–30 m thick and several hundred meters wide that cuts into and through a laterally continuous thick sandstone sheet at the top of a coarsening-upward succession of the HS (1–3) facies association (Figs. 8, 9). The sandstone body is laterally continuous across outcrop MBSE-17 but is not present at section MB-17, which is $\sim$ 2 km north (Fig. 1B). The basal CBS erosional surface has a relief of up to 10 m, and lower contacts with all HS facies and the MSD facies (Fig. 10). The upper contact of this facies with the overlying Mackellar Fm is sharp and horizontal.

This facies occurs in multistoried, multilateral sand-filled channel-form bodies displaying nonsequential, lateral compensational stacking patterns (Fig. 9). Individual channels are meter-scale thick and tens of meters wide, trough-shaped in cross section, and are filled by either vertical or downstream accretion dipping to the east. Channels are truncated by the bases of overlying channel bodies. Channel stacking is nonsequential and disorganized, with some aggradation. This facies is composed of well-sorted, medium- to very coarse-grained quartz sandstone, with minor occurrences of conglomerate lenses and beds (Fig. 9). Mudrocks were not observed in the sandstone bodies. Very rare pebble- and small-cobble-size clasts occur throughout the sandstones. Those clasts have lithologies similar to clasts observed in both diamictite facies (HS1 and MSD). Sedimentary structures are almost exclusively 0.15–1.5-m-thick sets of

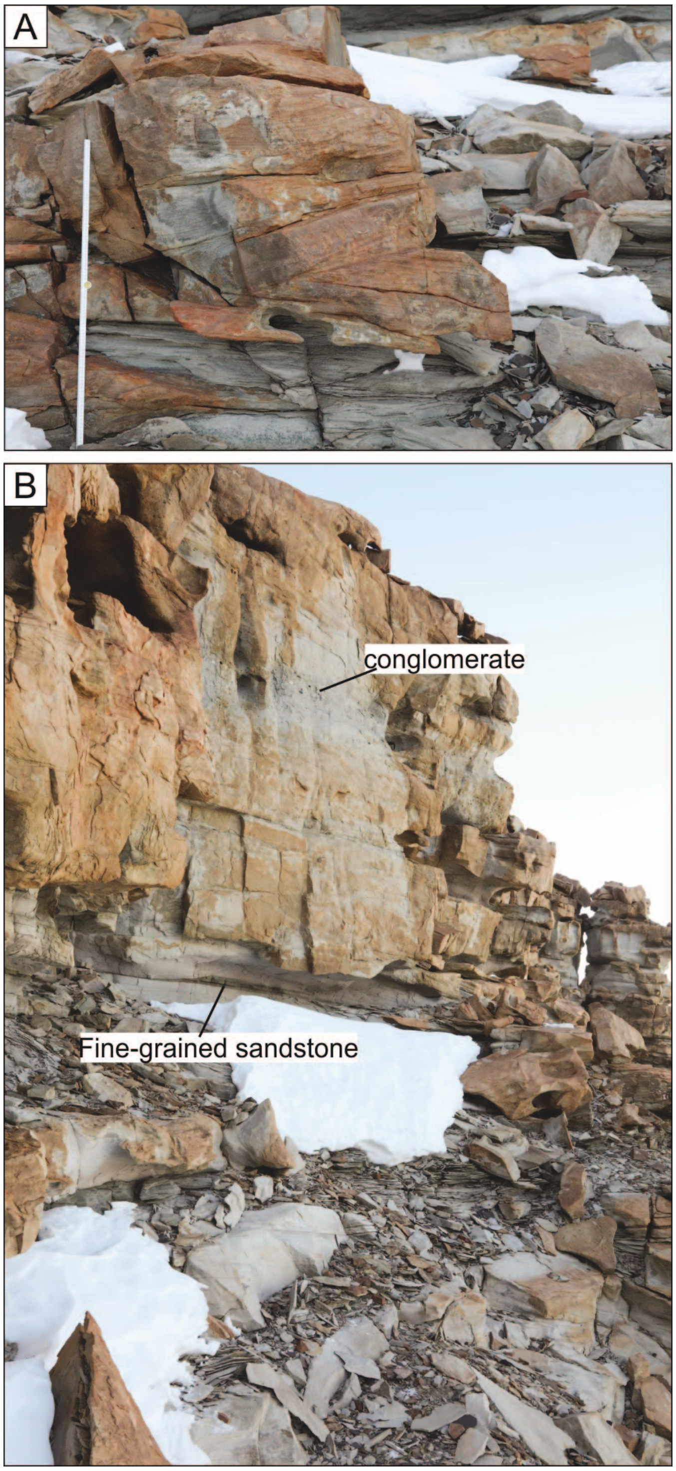

FIG. 9.—Photographs of the Cross Bedded Sandstone (CBS) facies at section MBSE-17 on Mt. Butters. **A)** An example of low-angle and trough cross-bed sets in this facies. Measuring stick is 1 m long. **B)** Photograph of facies in outcrop, noting occurrences of minor lithologies.

low-angle stratification and trough cross-beds (Fig. 9A). Thin beds with asymmetrical ripples also occur but are rare.

Adjacent to the described section (MBSE-17), the edge of the channel-form body appears to extend across the top of the underlying strata as a wing-like extension (Fig. 8A). Channel-form sandstone bodies occur in the wing. These bodies appear to transition laterally into other thick sandstones with channelized bases. Most notably, the contact between the channelized sandstones in the wing and the underlying HS facies appears to be sharp

CBS Interpretation.—The CBS facies in the Pagoda Fm was deposited by strong, tractive, confined flow as indicated by the occurrence of the basal erosion surface and the internal channel bodies filled by downstream-accreting bar forms and cross-stratification. The trough shape of the internal sandstone-filled channels and their multistoried and multilateral characteristics suggest that the channels were stationary during flow in the channels and that they did not migrate until channel switching occurred and new channels formed as older channels filled and were abandoned (Friend 1983). The occurrence of low-angle stratification and meter-scale trough cross beds organized into downstream-accreting bodies with massive bedded to lenticular gravels suggest high flow velocities. Such features are characteristic of highly dynamic systems where aggradation in channels likely forced channel switching to adjacent areas on the depositional surface. The occurrence of this facies association on top of unconfined coarsening-upward HS (1–3) facies association and the occurrence of wings that appear as a continuation of the HS (1–3) coarsening-upward succession suggest that the CBS facies formed as part of a HS–CBS larger-scale dispersal system. The presence of wings also suggests that parts of the CBS system were unconfined and represent "overbank" deposition on surfaces in areas between channels. Together, these patterns are most characteristic of an unconfined, distributive setting (Funk et al. 2012). This unit is similar to some grounding-line fan systems that authors have called subaqueous outwash fans (Visser et al. 1987; Thomas and Chiverrell 2006; Rose 2018).

Whether this facies was deposited subaerially or subaqueously is unclear. However, the CBS sandstone body does not contain evidence for shallow-water wave reworking, pedogenesis, or subaerial exposure, whereas facies both below and above this facies represent subaqueous deposition below normal wave base, and likely below storm wave base. Therefore, a subaqueous setting seems likely.

DEPOSITIONAL MODEL

Most of the Pagoda Fm in the Shackleton Glacier Area is composed of massive diamictites (facies MSD) that likely formed in glacier-proximal to glacier-intermediate environments, at depths largely below normal wave base, through a variety of glaciogenic and glacially influenced processes. These massive diamictites are also conformably overlain by, and interstratified with, grounding-line fan deposits (facies associations LS, HS, and CBS). These glacially derived lithologies are conformably succeed by prodeltaic, fine-grained facies of the Mackellar Fm.

Evidence for the grounded advance of a glacier(s) in the Shackleton Glacier region is present at base of the MSD facies at both Mt. Butters sites (MB-17 and MBSE-17) and at Mt. Munson (MM-17). The lower contact of the MSD facies is not exposed at Reid Spur, so similar inferences cannot be made for that locality. No conclusive evidence for subglacial deformation or erosion was observed higher in the Pagoda Fm at any site examined, though a subglacial origin for the MSD facies cannot be wholly ruled out. This advance was likely made by a glacier whose thickness exceed 100 m and flowed from north to south across the Shackleton Glacier region. The advance would have come from the direction of the present Ross Sea and crossing the TAB's margins perpendicular to the elongate trend of TAB (See discussion in prior section; Fig. 11D). This observation, along with other data from the TAB, strongly suggest that there were at least two ice centers in Antarctica during the Permian, one located on the East Antarctica craton and one in present day West Antarctica (Isbell 2010).

When the glacier margin retreated from the Mt. Butters, Mt. Munson, and Reid Spur sites, the deposition of glacier-proximal deposits was

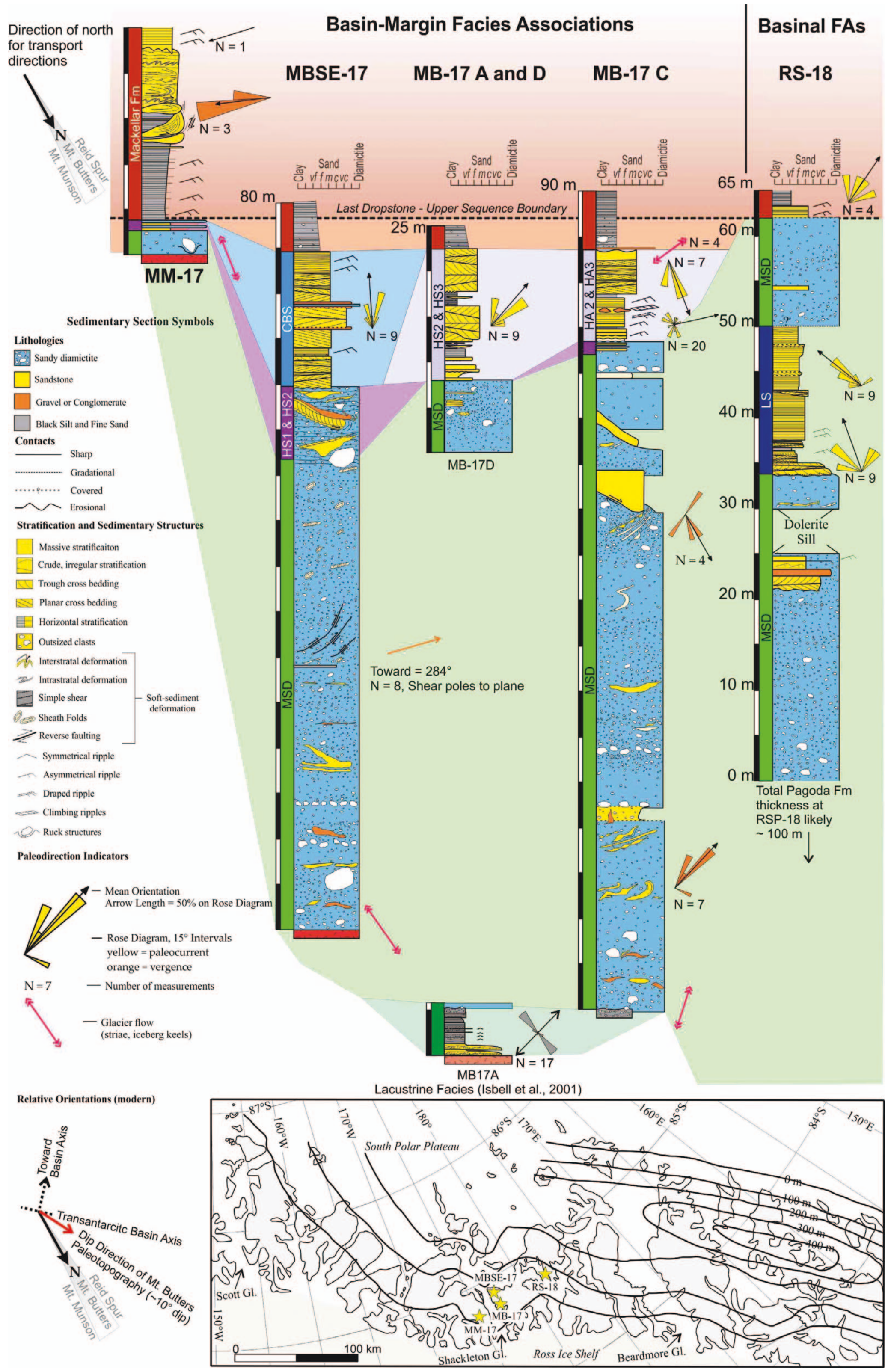

FIG. 10.—Sedimentary logs and paleotransport directions from sites described in this study. Paleotransport directions are plotted to align with the maps of modern Transantarctic Mountains presented in this study, so that north is toward the bottom of the page and varies by geographic position (see inset map). Details of paleotransport measurements are available in Table 2. MM-17 is Mt. Munson, MB-17(A–C) is Mt. Butters 1, MBSE-17 is Mt. Butters 2, and RS-18 is Reid Spur. Lithologies are grouped by their interpreted facies or facies association. Colored bars next to each log are used to indicate the distribution of facies associations in these sections, and colored areas in between sections show interpretation of each facies extent outside the section. Dark green corresponds to the localized lacustrine facies of the Pagoda Fm at Mt. Butters described by Isbell et al. (2001). Bright green represents the Massive Sandy Diamictite (MSD) facies association. Different shades of purple represent grouping of the Heterogenous Sandy facies association (HS1, stratified diamictite; HS2, chaotic sandstones; HS3, stratified sandstones). The inset map shows the location of each section and isopachs of the Pagoda Fm in the Beardmore Sub-basin from Isbell et al. (2008c). Light blue represents the Cross Bedded Sandstone facies (CBS). Dark blue represents the Laminated Sandstone facies association (LS). Red represents the Mackellar Fm. The datum for these columns were chosen using the last evidence for glaciogenic sediments, either the uppermost outsized clast or diamictite, which is a marker that also serves as an upper sequence boundary.

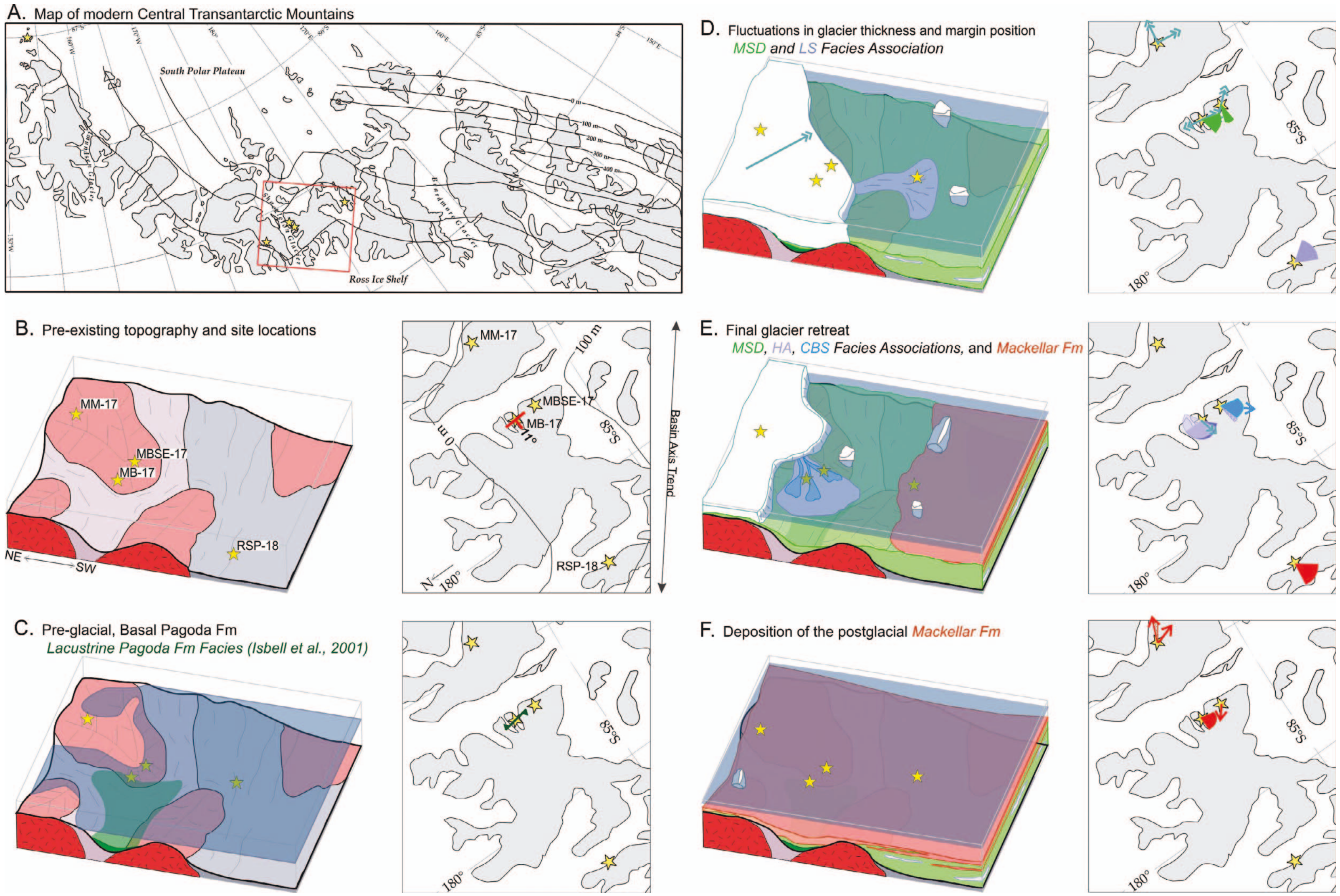

FIG. 11.—Box diagrams showing progressive phases of the depositional model for the Pagoda Fm and lowermost, glacially influenced Mackellar Fm in the Shackleton Glacier region, alongside maps showing the modern locations of the sites described in this study with transport orientations related to each part of the depositional model. See Table 3 for flow directions. **A)** Map of the modern central Transantarctic Mountains. Gray areas are approximate locations of nunatuk regions. Solid black lines are isopachs of the Pagoda Fm, copied from Isbell et al. (2008c). Red square indicates map area in Parts B–F. Note that the smaller map areas are rotated relative to the larger "map A." Yellow stars show site locations described in this study. **B)** Paleotopography of the Shackleton Glacier Area before deposition of the Pagoda Fm. Map shows strike and dip of granite surface underlying the Pagoda Fm at Mt. Butters site MB-17, corrected for modern structural conditions. This map also includes the Isbell et al. (2008c) isopach lines and derived basin-axis orientation for reference. **C)** Proposed depositional conditions for the lacustrine facies at the base of the Pagoda Fm at site MB-17 (Isbell et al. 2001). The green, double-sided arrow shown on the map shows the orientation of symmetrical (wave) ripple crests, which parallels the strike of the underlying basement. **D)** Proposed depositional conditions for Massive Sandy Diamictite (MSD) facies and Laminated Sands (LS) facies during retreat of the glacier out of the Shackleton Glacier area. On the map, purple wedge indicates range of flow direction in the LS facies, and green wedges indicate down-slope transport direction in the MSD facies. Blue double-headed arrows show glacier flow directions measured in this study. **E)** Proposed conditions during the deposition of the grounding-line fan represented by facies associations MSD, Heterogenous Sandy (HS), Cross-bedded Sands (CBS), and Mackellar Fm. The red wedge shows range of flow directions in the Mackellar Fm, blue and purple show the range of flow direction for the CBS and HS flow directions, respectively, and the blue arrow indicates the mean flow direction of the CBS facies at site MBSE-17. **F)** Proposed conditions during the deposition of the lower Mackellar Fm.

initiated. The massive diamictite (MSD) facies that dominated the Pagoda Fm at Mt. Butters and Reid Spur (RSP-18) was likely deposited through a combination of glaciogenic depositional processes characteristic of (*sensu lato*) glaciomarine settings, a combination of settling from suspension of neritic sediments, plume sedimentation from subglacial and englacial jets, as well as iceberg sedimentation and mixing. The prevalence of plume sedimentation and lack of hyperpycnal (under-) flow indicate that the water in the TAB was likely either marine or brackish. It should be noted that the TAB did not have a shelf, in the formal sense, as it was a trough-shaped basin that was not directly connected to the open ocean.

The Shackleton Glacier region during the Cisuralian was not an open shelf, but a near-coast setting with ample topographic relief, and water depths below normal wave base, such as St. George's Bay, Newfoundland (Sheppard et al. 2000). Ultimately, many of these sediments were likely remobilized by gravity-driven slides, slumps, and flows. This is especially true at the Mt. Butters site, where the vergence of soft-sediment deformation features in the MSD facies follow the local paleotopographic slope (Fig. 11B, E). Soft-sediment deformation caused by mass-transport deposits (facies HS) in bedded diamictites at Mt. Butters shows that the diamictites were unconsolidated, water-saturated, and subject to resedimentation, suggesting relatively rapid deposition.

At Mt. Butters and Reid Spur, massive diamictites are interstratified with and overlain by grounding-line fan deposits in the form of the LS, HS, and CBS facies associations. The stacked density flows (facies LS) at Reid Spur represent the medial to distal part of a fan, likely in relatively deep water. Flow direction in these sediments are towards the basin axis (Fig. 11D), suggesting that the basin geometry controlled topography in this area. On the other hand, the fan deposits at Mt. Butters are more proximal to the glacier margin. The laminated diamictites, reactivation surfaces, and storm-wave deposits in the fan at the top of the Mt. Butters section (MB-17 and MBSE-17) suggest that this fan was built gradually along a relatively stable margin and not during a single, catastrophic drainage event (Dowdeswell et al. 2016). The successions at Mt. Butters from the HS facies association through the CBS facies association represents either the progradation of one of these fans, a minor readvance associated with the deposition of the fan, or a combination of the two (Fig. 11E). The dispersed flow directions in the HS facies are characteristic of a fan, though their orientation broadly toward the north is away from the basin axis and opposed to glacier flow directions. Flow directions in the CBS facies are well clustered toward the southwest (Table 2, Fig. 11E). Influence of the paleotopographic slope at Mt. Butters and the radial nature of fan geometries are the most likely cause from these seemingly antagonistic flow directions (Fig. 11E). The orientation of the ice front would have also likely been influenced by this topography.

STRATIGRAPHIC FRAMEWORK

Basin-Margin vs. Basinal Facies Associations

Isbell et al. (2008c) described two generalized facies association of the Pagoda Fm: one that occurs in basinal settings and another that occurs along the basin margins. The sites described in this study from Mt. Munson and Mt. Butters in the Pagoda Fm are characteristic of the Basin Margin FA, because they are relatively thin successions ($<$ 100 m) and have evidence for subglacial erosion in the form of polished and striated bedrock (MBSE-17 and MM-17), and subglacially sheared lacustrine sediments (MB-17; Isbell et al. 2001). The site at Reid Spur (RSP-18) is also most characteristic of the Basin Margin FA, because diamictite facies there are thick and unstratified and has a poorly sorted matrix, suggesting plume sedimentation and gravity-driven redeposition. However, this section also likely represents a transition between the two facies associations. This is indicated by the LS facies at this site, which is attributable to the mid- to distal part of a grounding-line fan, and by the inferred thickness of the Pagoda Fm at Reid Spur ($\sim$ 100 m), which is the same as the transition thickness between Isbell et al. (2008c)'s two FAs.

Effects of Topography

The transport directions in these successions strongly suggest that paleotopography (relief on the Maya Erosional Surface) played a significant role in the deposition of the Pagoda in the Shackleton Glacier region. The influence of topography is particularly evident in the section MB-17 (Fig. 11). The surface of the basement at MB-17 dips toward the west at 11° (Figs. 4, 11B; Appendix A). Wave-ripple crests in facies BFG are parallel to the strike of the basement surface at MB-17 (Fig. 11C), suggesting that the paleotopography created by this surface was sufficient to affect and orient wave action. The transport directions of slumping and other gravity-driven processes in facies MSD at both sites MB-17 and MBSE-17 are also generally towards the west (Figs. 10, 11D), following the same slope. Flow directions in the grounding-line fan facies associations (HS and CBS) have a wide spread ranging from the southwest toward the east. However, in the HS facies association at MBSE-17, gravity-driven transport is still towards the west (Figs. 10, 11E). The south-southeast flow directions in the turbidite facies (LS) at site RSP-18 do not align with the flow direction at Mt. Butters, suggesting that those facies have a separate origin than the Mt. Butter's grounding line fan(s) (Figs. 10, 11D).

Paleotopographic control on the deposition of Pagoda Fm and Mackellar Fm has been noted by authors throughout the TAB (Lindsay 1970b; Barrett 1972; Isbell et al. 1997a, 2008c; Cornamusini et al. 2017). In previous studies, ice-flow directions (usually striae on bedrock or clast pavements) have often been combined with other transport directions in the Pagoda Fm to infer a generalized transport direction. However, recent work in modern, high-relief, glaciated landscapes has shown that the relationship between glacier flow directions, other transport directions, and topography can be used to infer the thickness of the glacier relative to the magnitude of relief on the landscape (Landvik et al. 2014). In other words, whether or not a glacier "follows" the underlying topography is a function of the glacier's thickness. Therefore, indicators of glacier flow should be considered separately from other transport directions.

The ice-flow directions below the Pagoda Fm in the Shackleton Glacier region are oriented generally northwest to southeast at Mt. Butters and Mt. Munson (Fig. 11D). Though none of the striae observed during this study had unidirectional indicators, previous workers in this area have found glacially carved features in the basement underlying the Pagoda Fm that show glacier flow was basin-ward (toward the south) or along the basin axis (toward the southeast) (Appendix A). These uniform flow directions on both a paleotopographic high (MM-17) and paleotopographic low (MB-17 and MBSE-17) suggest that the glacier, when it created these striae, was sufficiently thick to "overtop" the pre-existing topography in the Shackleton Glacier Area. Based on the difference in Pagoda Fm thickness, the local relief between site MB-17 (Mt. Butters) and MM-17 (Mt. Munson) was at least 85 m, and the onlapping of the Mackellar Fm onto basement in this area suggests that localized relief may have exceeded 100 m (Seegers 1996; Isbell et al. 1997a; Seegers-Szablewski and Isbell 1998). This scale of relief is on the scale of large hills. The topographic prominence of subglacial features on the scale of 100 m is considered negligible in studies of modern ice-sheet margins (e.g., Lindbäck and Pettersson 2015; Cooper et al. 2019), but would likely perturb or redirect the flow of relatively thin glaciers.

This discussion is all to say that the thickness of the glacier that created these striae more likely than not greatly exceeded the thickness of local topographic relief ($\sim$ 100 m), and that flow was most likely toward the center of the TAB. This inference suggests that the glacier was more likely an ice cap or ice sheet than an alpine glacier.

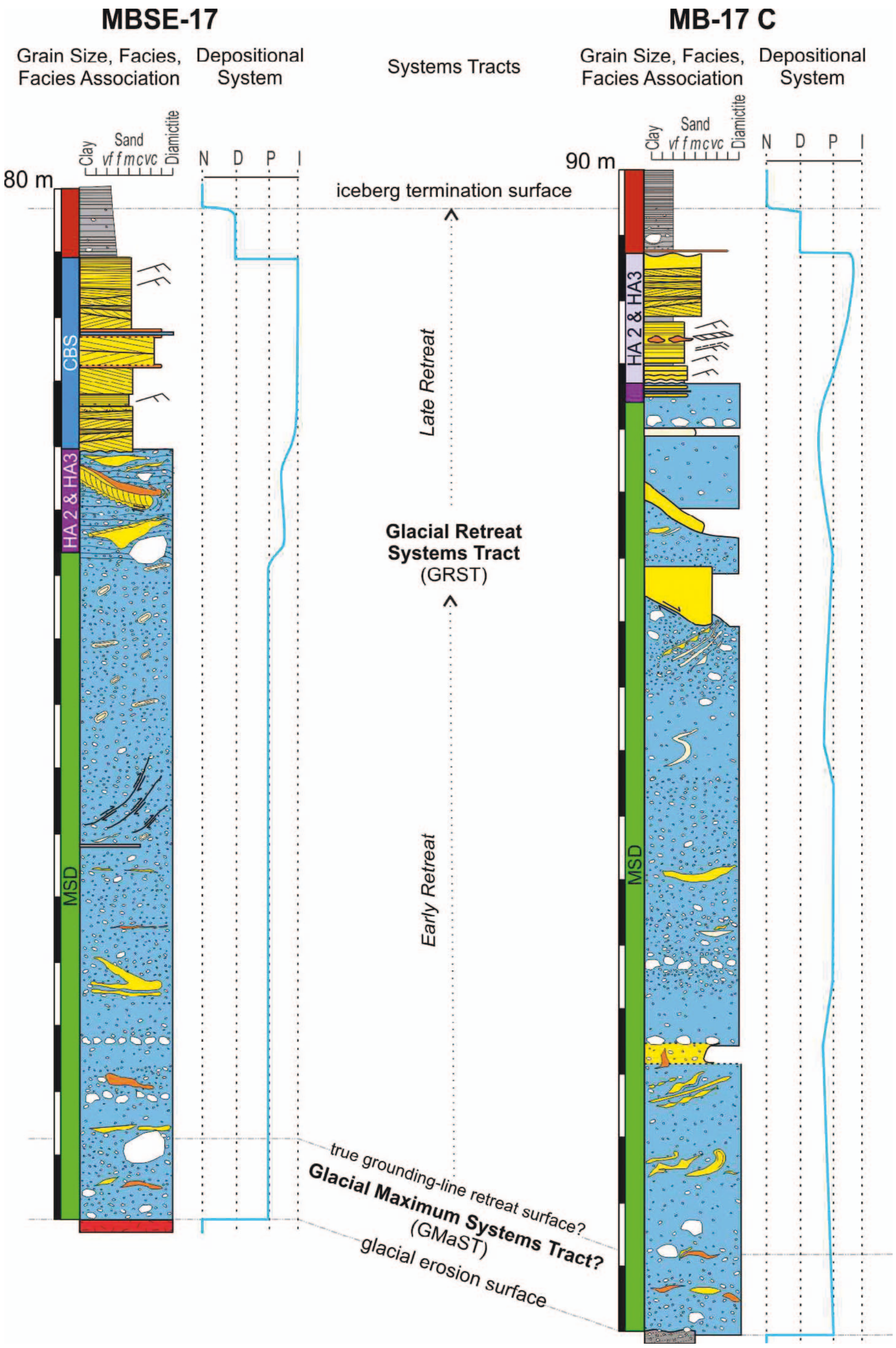

FIG. 12.—Glacial sequence stratigrapahy of the Mt. Butters sections, after Powell and Cooper (2002) and Rosenblume and Powell (2019). The depositional systems are defined as N, nonglacial; D, glacier distal; P, glacier proximal; and I, ice contact.

Glacial Systems Tracts

In this study, the sequence stratigraphy of the Pagoda Fm in the Shackleton Glacier region can be considered only at Mt. Butters, because that is the only location where the authors were able to measure complete sections. Since the Mt. Butters locations are basin-marginal successions (Fig. 11), this analysis of glacial sequence stratigraphy should not be considered applicable to basinal successions of the Pagoda Fm. The Pagoda Fm at Mt. Butters is unique in the TAB because it contains only a single glacial sequence as defined by Powell and Cooper (2002) and Rosenblume and Powell (2019) (Fig. 12). The sequence described in this paper is bounded at its base by a surface of glacial erosion (defined by striae on bedrock and the deformation of underlying lacustrine sediments (see Isbell et al. 2001) and at its top by an iceberg termination surface (defined by the final outsized clast in the section). Since the Pagoda Fm in this location is overlain by the nonglacial Mackellar Fm, there is no true maximum retreat surface beyond the iceberg termination surface (i.e., the last dropstone in the lower Mackellar Fm). Most of the succession likely represents a glacial-retreat systems tract, though there is likely some fraction of the massive diamictite facies above the erosional surface that is more likely to have been subglacially deposited and would therefore represent a glacial-maximum systems tract. The transition between those two systems tracts would be defined by a grounding-line retreat surface.

This sequence is most consistent with Rosenblume and Powell (2019)'s Type I "idealized glacial sequence," which is a model developed to reflect a sedimentation sequence deposited during the retreat of a relatively warm subpolar glacier with a glacial erosion surface as a lower sequence boundary and sufficient meltwater for the development of grounding-line fans. This sequence model was developed based on upper Miocene sediments from the Ross Sea region of Antarctica (Rosenblume and Powell 2019), whose climatic and geology were likely reasonably similar to the TAB during the Permian. The Type I idealized sequence is interpreted to represent a dynamic climatic glacial system with very high erosion rates and debris fluxes, which is consistent with the depositional model presented for the Pagoda Fm in this paper.

DISCUSSION

This study finds that most of sediments in the Pagoda Fm in the Shackleton Glacier region were deposited during the retreat of a temperate to "mild" subpolar glacier. The key indicators for this retreat include the presence of grounding-line fan systems, ample evidence for plume sedimentation and rapid deposition, as well as abundant glacially transported clasts with a wide size range made of local basement lithologies. This glacier had a subaqueous terminus during the deposition of the Pagoda Fm in the Shackleton Glacier area, either in a marine or a brackish setting.

One of the ultimate goals of the study of LPIA glaciogenic sediments is to infer the "type" and distribution of glaciation experienced in any given basin. Glacier "type" typically refers to the glacier's thermal regime and its size (i.e., ice sheet, ice cap, or ice field). Such characteristics of glaciers are controlled by many factors but generally tie back into climate and geologic setting. Glaciogenic sedimentary deposits are often used to infer the thermal regime of their parent glacier (Dowdeswell et al. 2016; Kurjanski et al. 2020). Recent studies all agree that glaciogenic deposits in the TAB are most likely the result of transport and deposition by temperate or "mild" subpolar glaciers, largely because grounding-line fans are common in the Pagoda Fm and its equivalents, which suggest that the TAB glaciers released an abundance of meltwater (Isbell et al. 2008c; Isbell 2010; Koch and Isbell 2013; Cornamusini et al. 2017).

The presence of subaqueous fan deposits interspersed in the massive diamictite facies of the Pagoda Fm in the Shackleton Glacier area suggests that the glacier had an active, persistent, and organized subglacial hydrologic system, and that during its retreat the glacial margin was stationary for at least a few years at a time to create grounding-line fans (Cowan and Powell 1991; Hunter et al. 1996; Dowdeswell et al. 2015, 2016). These inferences are also supported by the succession's stratigraphy, which is characteristic of a "Type I" ("mild" subpolar glacier with grounding-line-fan development) glacial systems tract (Rosenblume and Powell 2019). Whether the glacier responsible for the deposition of the Pagoda Fm in the Shackleton Glacier Region had more of a "mild subpolar" thermal regime, similar to modern glaciers in eastern Svalbard, or more of a truly "temperate" thermal regime, like modern glaciers of southern Alaska, is difficult to discern. To clarify likely thermal regime, additional glaciogenic successions and nonglacial paleoclimate indicators in the TAB should be examined. In either case, glaciers with mild thermal regimes and developed subglacial hydrological systems are far and away the more prolific producers and transporters of sediments, and that the sedimentary record is therefore biased towards them. The presence of deposits from temperate or mild subpolar glaciers does not mean the thermal regime of the glaciers were never cold-based or that there was not lateral variation in glacier thermal regime.

The unidirectional orientation of subglacial flow indicators, along with evidence to topographic relief exceeding $\sim$ 100 m in the Shackleton Glacier region, suggest that glacier thickness also exceeded 100 m during its maximum. Such observations do not allow an inference of maximum possible ice thickness. However, we can infer that the glacier was more likely part of an ice sheet or ice cap than an ice field or alpine glacier. The glacier also may have thinned substantially during its retreat and subsequent deposition of the Pagoda Fm in this area.

Throughout the TAB, Asselian–Sakmarian glaciogenic depositional environments were locally and regionally variable in part due to the inherent complexity of glacial processes and preservation potential, but also due to the topography of the pre-existing landscape. Most studies of glaciogenic rocks in the TAB note up to several hundred meters of topographic relief on the underlying basement that is not wholly "filled" by glacial sediments and continued to influence postglacial sediment deposition (Isbell et al. 1997a). Studies of both modern (e.g., Lawson (1979)) and ancient (e.g., Cornamusini et al. (2017)) glacial sedimentary systems have observed how topographic effects can result in seemingly contradictory flow directions. This study is another example. Transport directions at all of the sites in this study appear contradictory, unless paleotopography and processes that created each feature are considered (Fig. 11). For example, at Mt. Butters the flow directions of Permian glaciers in the TAB appears to be from north to south, while the transport directions of gravity-driven deposits and flow directions in the grounding-line fan are perpendicular to that (Fig. 11D, E). If averaged together, these flow directions would imply general transport toward the southwest, when the most likely scenario was that the mass- and current-transported deposits followed a paleotopographic slope and the glacier did not.

The Pagoda Fm in the Shackleton Glacier region likely represents a single glacial–interglacial cycle, stratigraphically represented by a single glacial sequence. In this context, the phrase "glacial–interglacial cycle" refers to the advance of a glacier into the basin and its whole retreat out of the basin, which is stratigraphically defined by a surface of glacial retreat. This is not to say that the position of the glacier margin did not fluctuate during that cycle, but that only one grounded erosional surface is present in the study area and only one surface of glacier retreat (Powell and Cooper 2002; Rosenblume and Powell 2019). No instances of a grounded readvance over any of the sections examined in this study were observed beyond the basal erosional surfaces. As previously discussed, the processes and environments responsible for the extensive deposition of the massive, glaciogenic diamictite facies were likely diverse and largely subaqueous. The preservation of such sediments is most probable if they were deposited during the final retreat phase with no subsequent advances over the area (Kurjanski et al. 2020). This is especially true in a basin-marginal position in a basin like the TAB that was trough-shaped and not exposed to open-marine conditions. Evidence for glacier readvance above the basal erosional surface of the Pagoda Fm does exist at other Pagoda Fm outcrops in the TAB, including in the Beardmore Sub-basin (Lindsay 1970a; Miller 1989; Koch and Isbell 2013). This evidence typically occurs in thicker, basinal facies association which are likely areas with higher accommodation than the basin margins.

The flow directions and facies analyses from this study strongly support the hypothesis that an ice center was positioned inboard of the Panthalassan margin of Antarctica (an area that is now Marie Byrd Land) during the Asselian–Sakmarian (Fig. 2B, ice center "q"). The presence of such an ice sheet is a relatively new hypothesis that was first proposed by Isbell (2010) and Isbell et al. (2008c) based on transport directions in South Victoria Land. In recent publications, this proposed ice center on the Panthalassan side of the TAB has been inconsistently included (Fielding et al. 2008c; Isbell et al. 2012; Montañez and Poulsen 2013) and excluded (Fielding et al. 2010; Craddock et al. 2019) from LPIA ice-center reconstructions. Evidence from this study and Isbell (2010) shows that an ice center should be included on the non-cratonic edge of the TAB in reconstructions including the Gzhelian–Sakmarian, an interval also referred to as "Event 5"(López-Gamundí et al. 2021), and Australian "P1" (Fielding et al. 2008b). Ice-flow directions elsewhere in the TAB clearly indicate that glaciers also flowed into the TAB off of the East Antarctic Craton and along the TAB's basin axis toward the Wisconsin and Ohio ranges (Fig. 2B, ice center "r"). The multiple ice centers contributing to sedimentation in the TAB may not have been synchronous in their advances and retreats throughout the LPIA. This additional evidence for an ice center over Marie Byrd Land is important because it helps to explicate the hypothesis that glaciation during the LPIA consisted of asynchronous, discrete ice centers and not a single, large ice sheet centered over Antarctica (Isbell et al. 2012; Montañez and Poulsen 2013) (Fig. 2B). Inferences made from glaciogenic and glacially influenced sediments ("near-field" records) can be tied to global and "far-field" records of climate change from the $\sim$ 80 Myr of the LPIA to approach a holistic understanding of the effects that the onset, duration, and ultimate collapse of a global icehouse-influenced Earth, both geologically and biologically (Montañez et al. 2007; Rygel et al. 2008; Soreghan et al. 2019).

CONCLUSIONS

The Pagoda Fm in the Shackleton Glacier region is glaciogenic and was deposited in a basin-marginal subaqueous setting, by a glacier with a temperate or mild subpolar thermal regime. The dominant lithology in the Pagoda Fm here is massive, sandy, clast-poor diamictite. The depositional processes governing these diamictites were subaqueous glacial processes in a marine or brackish setting; likely a combination of mass transport, iceberg rain-out, iceberg scouring, plume sedimentation, and subglacial till deposition. Current-transported sands and stratified diamictites in the Pagoda Fm were deposited as part of grounding-line fan systems. In the Shackleton Glacier region, all glaciogenic sediments in the Pagoda Fm were likely deposited during the retreat phase of a single glacial sequence. The transport directions and thicknesses of strata along the TAB margin were strongly controlled by topographic relief on the underlying erosional surface. Glacier flow directions (towards the south and southeast) and trends in Pagoda Fm thicknesses in the Shackleton Glacier Area support the hypothesis that an ice center was present toward the Panthalassan margin of East Antarctica (Marie Byrd Land) during the LPIA.

SUPPLEMENTAL MATERIAL

Supplemental appendices are available from SEPM's Data Archive: https://www.sepm.org/supplemental-materials.

ACKNOWLEDGMENTS

This work would have been impossible without the hard work of all the people who made the 2017–2018 Shackleton Deep Field Camp such a success, including the talented people of the National Science Foundation, Antarctic Support Contract, Ken Borek Air, Petroleum Helicopters, Inc., New York Air National Guard, and the U.S. Air Force. Special thanks are owed to Edith Taylor and Rudolf Serbet for aiding in the field planning, Danny Uhlmann and Ted Grosgebauer for keeping us from tumbling off of cliffs, and to Patty Ryberg, Rudolf Serbert, Brian Atkinson, and Erik Gulbranson for their companionship and cooking in the deep field. Thanks also to Kate Pauls and Eduardo Rosa for their feedback on the manuscript. Funding for this research came from National Science Foundation OPP-1443557, EAR-1729219, and OISE-1559231 grants, the University of Wisconsin–Milwaukee Graduate Fellowships programs, the P.E.O. Scholar Awards Program, The American Federation of Mineralogical Societies, The Wisconsin Geological Society, University of Wisconsin–Milwaukee (RGI grant), and the University of Wisconsin–Milwaukee Department of Geosciences. And finally, thanks are due to Fernando Vesely and an anonymous reviewer for their thoughtful comments and suggestions that improved this manuscript.

REFERENCES

Aitchison, J.C., Bradshaw, M.A., and Newmann, L., 1988, Lithofacies and origin of the Buckeye Formation: late Paleozoic glacial and glaciomarine sediments, Ohio Range, Transantarctic Mountains, Antarctica: Palaeogeography, Palaeoclimatology, Palaeoecology, v. 64, p. 93–104.

Allmendinger, R.W., Cardozo, N., and Fisher, D.M., 2012, Structural Geology Algorithms: Vectors and Tensors in Structural Geology: Cambridge University Press, 302 p.

Anderson, J.B., Kurtz, D.D., Domack, E.W., and Balshaw, K.M., 1980, Glacial and glacial marine seidment of the Antarctic continental shelf: Journal of Geology, v. 88, p. 399–414.

Askin, R.A., 1998, Floral trends in the Gondwana high latitudes: palynological evidence from the Transantarctic Mountains: Journal of African Earth Sciences, v. 27, p. 12–13.

Askin, R.A., Barrett, P.J., Kohn, B.P., and McPherson, J.G., 1971, Stratigraphic sections of the Beacon Supergroup (Devonian and older(?) to Jurassic) in south Victoria Land, *in* Barrett, P.J., ed., Antarctic Data Series No. 2: Wellington, Victoria University.

Assine, M.L., De Santa Ana, H., Veroslavsky, G., and Vesely, F.F., 2018, Exhumed subglacial landscape in Uruguay: erosional landforms, depositional environments, and paleo-ice flow in the context of the late Paleozoic Gondwanan glaciation: Sedimentary Geology, v. 369, p. 1–12.

Babcock, L.E., Isbell, J.L., Miller, M.F., and Hasiotis, S.T., 2002, New late Paleozoic conchostracan (Crustacea: Branchiopoda) from the Shackleton Glacier Area, Antarctica: Age and paleoenvironmental implications: Journal of Paleontology, v. 76, p. 70–75.

Barrett, P.J., 1972, Late Paleozoic glacial valley at Alligator Peak, Southern Victoria Land, Antarctica: New Zealand Journal of Geology and Geophysics, v. 15, p. 262–268.

Barrett, P.J., and McKelvey, B.C., 1981, Permian tillites of southern Victoria Land, Antarctica, *in* Hambrey, M.J., and Harland, W.B., eds., Earth's pre-Pleistocene Glacial Record: Cambridge, Cambridge University Press, p. 233–236.

Barrett, P.J., Elliot, D.H., and Lindsay, J.F., 1986, The Beacon Supergroup (Devonian–Triassic) and Ferrar Group (Jurassic) in the Beardmore Glacier area, Antarctica, *in* Turner, M.D., and Splettstoesser, J.F., eds., Geology of the central Transantarctic Mountains: American Geophysical Union, Antarctic Research Series, p. 339–428.

Batchelor, C.L., and Dowdeswell, J.A., 2015, Ice-sheet ground-zone wedges (GZWs) on high-latitude continental margins: Marine Geology, v. 363, p. 65–92.

Batterson, M., and Sheppard, K., 2000, Deglacial history of northern St. George's Bay, western Newfoundland: Newfoundland Department of Mines and Energy, Geological Survey of Newfoundland, Current Research, v. 1, p. 33–47.

Benn, D.I., 1996, Subglacial and subaqueous processes near a glacier grounding line: sedimentological evidence from a former ice-dammed lake, Achnasheen Scotland: Boreas, v. 25, p. 23–36.

Bennett, M.R., Hambrey, M.J., and Huddart, D., 1997, Modification of clast shape in high artic glacial environments: Journal of Sedimentary Research, v. 67, p. 550–559.

Bindschadler, R., Vornberger, V., Fleming, A., Fox, A., Mullins, J., Binnie, D., Paulsen, S.J., Granneman, B., and Gorodestzky, D., 2008, The Landsat image mosaic of Antarctica: Remote Sensing of Environment, v. 112, p. 4214–4226.

Cardozo, N., and Allmendinger, R.W., 2013, Spherical projections with OSXStereonet: Computers & Geosciences, v. 51, p. 193–205.

Coates, D.A., 1985, Late Paleozoic glacial patterns in the central Transantarctic Mountains, Antarctica, *in* Turner, M.D., and Splettstoesser, J.F., eds., Geology of the Central Transantarctic Mountains: American Geophysical Union, Antarctic Research Series, p. 325–338.

Collinson, J.D., and Mountney, N., 2019, Sedimentary Structures: Edinburgh, Academic Press, 340 p.

Collinson, J.W., Isbell, J.L., Elliot, D.H., Miller, M.F., and Miller, J.M.G., 1994, Permian–Triassic Transantarctic basin, *in* Veevers, J.J., and Powell, C.M., eds., Permian–Triassic Pangean basins and Foldbelts along the Panthalassan Margin of Gondwanaland: Geological Society of America, Memoir 184, p. 173–222.

Collinson, J.W., Hammer, W.R., Askin, R.A., and Elliot, D.H., 2006, Permian–Triassic boundary in the central Transantarctic Mountains, Antarctica: Geological Society of America, Bulletin, v. 118, p. 747–763.

Cooper, M.A., Jordan, T.M., Schroeder, D.M., Siegert, M.J., Williams, C.N., and Bamber, J.L., 2019, Subglacial roughness of the Greenland Ice Sheet: relationship with contemporary ice velocity and geology: The Cryosphere, v. 13, p. 3093–3115.

Cornamusini, G., Talarico, R.M., Simonette, C., Spine, A., Olivetti, V., and Woo, J., 2017, Upper Paleozoic glacigenic deposits of Gondwana: stratigraphy and paleoenvironmental significance of a tillite succession in Northern Victoria Land (Antarctica): Sedimentary Geology, v. 358, p. 51–69.

Cowan, E.A., and Powell, R.D., 1991, Ice-proximal sediment accumulation rates in a temperate glacial fjord, south-eastern Alaska, *in* Anderson, J.B., and Ashley, G.M., eds., Glacial Marine Sedimentation: Paleoclimatic Significance: Geological Society of America, Special Paper 261, p. 61–73.

Craddock, J.P., Ojakangas, R.W., Malone, D.H., Konstantinou, A., Mory, A.J., Bauer, W., Thomas, R.J., Affinati, S.C., Pauls, K.N., Zimmerman, U., Botha, G., Rochas-Campos, A., Dos Santos, P.R., Tohver, E., Riccomini, C., Martin, J., Redfern, J., Horstwood, M., and Gehrels, G., 2019, Detrital Zircon Provenance of Permo-Carboniferous Glacial Diamictites across Gondwana: Earth-Science Reviews, v. 192, p. 285–316.

Crowell, J.C., and Frakes, L.A., 1972, Late Paleozoic glaciation: Part V, Karoo Basin, South Africa: Geological Society of America, Bulletin, v. 83, p. 2887–2919.

Crowell, J.C., and Frakes, L.A., 1975, Late Paleozoic glaciaition, *in* Campbell, K.S.W., ed., Gondwana Geology: Papers Presented at the Third Gondwana Symposium Canberra, Australia, 1973: Canberra, Australia, Australian National University Press, p. 313–331.

Dasgupta, P., 2006, Facies characteristics of Talchir Formation, Jharia Basin, India: implications for initiation of Gondwana sedimentation: Sedimentary Geology, v. 185, p. 59–78.

Demet, B.P., Nittrouer, J.A., Anderson, J.B., and Simkins, L.M., 2019, Sedimentary processes at ice sheet grounding-zone wedges revealed by outcrops, Washington State (USA): Earth Surface Processes and Landforms, v. 44, p. 1209–1220.

Dietrich, P., Franchi, F., Setlhabi, L., Prevec, R., and Bamford, M., 2019, The nonglacial diamictite of Toutswemogala Hill (lower Karoo Supergroup, central Botswana): implications of the extent of the Late Paleozoic Ice Age in the Kalahari–Karoo Basin: Journal of Sedimentary Research, v. 89, p. 1–15.

Dietrich, P., and Hoffmann, A., 2019, Ice-margin fluctuation sequences and grounding zone wedges: the record of the Late Palaeozoic Ice Age in the eastern Karoo Basin (Dwyka Group, South Africa): The Depositional Record, v. 5, no. 2, p. 247–271.

Domack, E.W., 1983, Facies of Late Pleistocene glacial–marine sediments on Whidbey Island, Washington: an isostatic glacial–marine sequence, *in* Molina, B.F., ed., Glacial–Marine Sedimentation: Boston, Springer, p. 535–570.

Domack, E.W., and Powell, C.M., 2018, Modern Glaciomarine Environments and Sediments, *in* Menzies, J., and van der Meer, J.J.M., eds., Past Glacial Environments: Elseveir, p. 105–158.

Domeier, M., and Torsvik, T.H., 2014, Plate tectonics in the late Paleozoic: Geoscience Frontiers, v. 5, p. 303–350.

Dowdeswell, J.A., Hambrey, M.J., and Wu, R., 1985, A comparison of clast fabric and shape in Late Precambrian and modern glacigenic sediments: Journal of Sedimentary Petrology, v. 55, p. 691–704.

Dowdeswell, J.A., Whittington, R.J., and Marienfeld, P., 1994, The origin of massive diamicton facies by iceberg rafting and scouring, Scoresby Sund, East Greenland: Sedimentology, v. 41, p. 21–35.

Dowdeswell, J.A., Hogan, K.A., Arnold, N.S., Mugford, R.I., Wells, M., Hirst, J.P.P., and Decalf, C., 2015, Sediment-rich meltwater plumes and ice-proximal fans at themargins of modern and ancient tidewater glaciers: Observations and modeling: Sedimentology, v. 62, p. 1665–1692.

Dowdeswell, J.A., Canals, M., Jakobsson, B.J., Todd, B.J., Dowdeswell, E.K., and Hogan, K.A., 2016, The variety and distribution of submarine glacial landforms and implications for ice-sheet reconstruction, *in* Dowdeswell, J.A., Canals, M., Jakobsson, B.J., Todd, B.J., Dowdeswell, E.K., and Hogan, K.A., eds., Atlas of Submarine Glacial Landforms: Modern, Quaternary and Ancient: Geological Society of London, Memoir 46, p. 519–552.

Dumas, S., and Arnott, R.W.C., 2006, Origin of hummocky and swaley cross-stratification: the controlling influence of unidirectional current strength and aggradation rate: Geology, v. 34, p. 1073–1076.

Eidam, E.F., Sutherland, D.A., Duncan, D., Kienholz, C., Amundson, J.M., and Motyka, R.J., 2020, Morainal bank evolution and impact on terminus dynamics during a tidewater glacier stillstand: Journal of Geophysical Research: Earth Surface, v. 125, no. 11, e2019JF005359.

Elliot, D.H., 1992, Jurassic magmatism and tectonism associated with Gondwanaland break-up: an Antarctic perspective, *in* Storey, B.C., Alabaster, T., and Pankhurst, R.J., eds., Magmatism and the Causes of Continental Break-Up: Geological Society of London, Special Publication 68, p. 165–184.

Elliot, D.H., 2013, The geological and tectonic evolution of the Transanatarctic Mountains: a review, *in* Hambrey, M.J., Barker, P.F., Barrett, P.J., Bowman, V., Davies, B., Smellie, J.L., and Tranter, M., eds., Antarctic Palaeoenvironments and Earth-Surface Processes: Geological Society of London, Special Publication 381, p. 7–35.

Elliot, D.H., Fanning, C.M., Isbell, J.L., and Hulett, S.R.W., 2017, The Permo-Triassic Gondwana sequence, central Transantarctic Mountains, Antarctica: zircon geochronology, provenance, and basin evolution: Geosphere, v. 13, p. 155–178.

Estrada, S., Läufer, A., Eckelmann, K., Hofmann, M., Gärtner, A., and Linnemann, U., 2016, Continuous Neoproterozoic to Ordovician sedimentation at the East Gondwana margin: implications from detrital zircons of the Ross Orogen in northern Victoria Land, Antarctica: Gondwana Research, v. 37, p. 426–448.

Evans, D.J.A., Phillips, E.R., Hiemstra, J.F., and Auton, C.A., 2006, Subglacial till: formation, sedimentary characteristics and classification: Earth-Science Reviews, v. 78, p. 115–176.

Eyles, C.H., 1987, Glacially influenced submarine-channel sedimentation in the Yakataga Formation, Middleton Island, Alaska: Journal of Sedimentary Petrology, v. 57, p. 1004–1017.

Eyles, C.H., 1988, A model for striated boulder pavement formation on glaciated, shallow-marine shelves: an example from the Yakataga Formation, Alaska: Journal of Sedimentary Petrology, v. 58, p. 62–71.

Eyles, C.H., and Lagoe, M.B., 1990, Sedimentation patterns and facies geometry on a temperate glacially-influenced continental shelf: the Yakataga Formation, Middleton Island, Alaska, *in* Dowdeswell, J.A., and Scourse, J.D., eds., Glacimarine Environments: Processes and Sediments: Geological Society of London, Special Publication 53, p. 363–386.

Fallgatter, C., and Paim, P.S.G., 2019, On the origin of the Itararé Group basal nonconformity and its implications for the late Paleozoic glaciation in the Paraná Basin, Brazil: Palaeogeography, Palaeoclimatology, Palaeoecology, v. 531, 108225.

Fedorchuk, N.D., Isbell, J.L., Griffis, N.P., Montañez, I.P., Vesely, F.F., Iannuzzi, R., Mundil, R., Yin, Q.-Z., Pauls, K.N., and Rosa, E.L., 2019, Origin of paleovalleys on the Rio Grande do Sul Shield (Brazil): implications for the extent of late Paleozoic glaciation in west-central Gondwana: Palaeogeography, Palaeoclimatology, Palaeoecology, v. 531, 108738.

Fielding, C.R., Sliwa, R., Holcombe, R.J., and Jones, A.T., 2001, A new palaeogeographic synthesis for the Bowen, Gunnedah and Sydney basins of eastern Australia, *in* Hill, K.C., and Bernecker, T., eds., Eastern Australasian Basins Symposium: A Refocused Energy Perspective for the Future: Victoria, Australia, Petroleum Exploration Society of Australia, Special Publication, p. 269–278.

Fielding, C.R., Frank, T.D., Birgenheier, L.P., Rygel, M.C., Jones, A.T., and Roberts, J., 2008a, Stratigraphic imprint of the late Palaeozoic ice age in eastern Australia: a record of alternating glacial and nonglacial climate regime: Geological Society of London, v. 165, p. 129–140.

Fielding, C.R., Frank, T.D., Birgenheier, L.P., Rygel, M.C., Jones, A.T., and Roberts, J., 2008b, Stratigraphic record and facies associations of the late Paleozoic ice age in eastern Australia (New South Wales and Queensland), *in* Fielding, C.R., Frank, T., and Isbell, J.L., eds., Resolving the Late Paleozoic Ice Age in Time and Space: Geological Society of America, Special Paper 441, p. 41–57.

Fielding, C.R., Frank, T.D., and Isbell, J.L., 2008c, The Late Paleozoic Ice Age: a review of current understanding and synthesis of global climate patterns, *in* Fielding, C.R., Frank, T.D., and Isbell, J.L., eds., Resolving the Late Paleozoic Ice Age in Time and Space: Geological Society of America, Special Publication 441, p. 343–354.

Fielding, C.R., Frank, T.D., and Isbell, J.L., eds., 2008d, Resolving the Late Paleozoic Ice Age in Time and Space: Geological Society of America, Special Publication 441, 354 p.

Fielding, C.R., Frank, T.D., Isbell, J.L., Henry, L.C., and Domack, E.W., 2010, Stratigraphic signature of the late Palaeozoic Ice Age in the Parmeener Supergroup of Tasmania, SE Australia, and inter-regional comparisons: Palaeogeography, Palaeoclimatology, Palaeoecology, v. 298, p. 70–90.

Frakes, L.A., and Crowell, J.C., 1969, Late Paleozoic glaciation: I, South America: Geological Society of America, Bulletin, v. 80, p. 1007–1042.

Frakes, L., Matthews, J., Neder, I., and Crowell, J., 1966, Movement directions in late Paleozoic glacial rocks of the Horlick and Pensacola Mountains, Antarctica: Science, v. 153, p. 746–749.

Frakes, L.A., Matthews, J.L., and Crowell, J.C., 1971, Late Paleozoic glaciation: Part III, Antarctica: Geological Society of America, Bulletin, v. 82, p. 1581–1604.

França, A.B., and Potter, P.E., 1988, Estratigrafia, ambiente deposicional e analise de reservatorio do Grupo Itarare (Permocarbonifero), Bacia do Parana (Parte 1): PETROBRAS, Boletim de Geociencias, v. 2, p. 147–191.

França, A.B., Winter, W.R., and Assine, M.L., 1996, Arenitos Lapa–Vila Velha; um modelo de trato de sistemas subaquosos canal–lobos sob influencia glacial, Grupo Itarare (C-P), Bacia do Parana: Revista Brasileira de Geociencias, v. 26, p. 43–56.

Friend, P.F., 1983, Towards the field classification of alluvial architecture or sequence, *in* Collinson, J.D., and Lewin, J., eds., Modern and Ancient Fluvial Systems, International Association of Sedimentologists, Special Publication 6, p. 345–354.

Funk, J.E., Slatt, R.M., and Pyles, D.R., 2012, Quantification of static connectivity between deep-water channels and stratigraphically adjacent architectural elements using outcrop analogs: American Association of Petroleum Geologists, Bulletin, v. 96, p. 277–300.

Gastaldo, R.A., Dimichele, W.A., and Pfefferkorn, H.W., 1996, Out of the icehouse into the greenhouse; a late Paleozoic analog for modern global vegetational change: GSA Today, v. 6, no. 10, p. 1–7.

Goodge, J.W., 2020, Geological and tectonic evolution of the Transantarctic Mountains, from ancient craton to recent enigma: Gondwana Research, v. 80, p. 50–122.

Goodge, J.W., and Fanning, M.C., 2016, Mesoarchean and Paleoproterozoic history of the Nimrod Complex, central Transantarctic Mountains, Antarctica: stratigraphic revisions andrelation to the Mawson Continent in East Gondwana: Precambrian Research, v. 285, p. 242–271.

Hallet, B., Hunter, L., and Bogen, J., 1996, Rates of erosion and sediment evacuation by glaciers: a review of field data and their implications: Global and Planetary Change, v. 12, p. 213–235.

Hambrey, M.J., 1994, Glacial Environments: Vancouver, University of British Columbia Press, 296 p.

Hambrey, M.J., and Glasser, N.F., 2003, Glacial sediments: processes, environments and facies, *in* Middleton, G.V., ed., Encyclopedia of Sediments and Sedimentary Rocks: Dordrecht, Kluwer Academic Publishers, p. 316–331.

Hambrey, M.J., and Glasser, N.F., 2012, Discriminating glacier thermal and dynamic regimes in the sedimentary record: Sedimentary Geology, v. 251–252, p. 1–33.

Hand, S.J., 1993, Palaeogeography of Tasmania's Permo-Carboniferous glacigenic sediments, *in* Findlay, R.H., Unrug, R., Banks, M.R., and Veevers, J.J., eds., Gondwana Eight: Assembly, Evolution and Dispersal: Rotterdam, A.A. Balkema, p. 459–469.

Hunter, L.E., Powell, R.D., and Lawson, D.E., 1996, Flux of debris transported by ice at three Alaskan tidewater glaciers: Journal of Glaciology, v. 42, p. 123–135.

Isbell, J.L., 1999, The Kukri Erosion Surface: a reassessment of its relationship to rocks of the Beacon Supergroup in the central Transantarctic Mountains, Antarctica: Antarctic Science, v. 11, p. 228–238.

ISBELL, J.L., 2010, Environmental and paleogeographic implications of glaciotectonic deformation of glaciomarine deposits within Permian strata of the Metschel Tillite, southern Victoria Land, Antarctica, *in* López-Gamundí, O.R., and Buatois, L.A., eds., Late Paleozoic Glacial Events and Postglacial Transgressions in Gondwana: Geological Society of America, Special Publication 468, p. 81–100.

ISBELL, J.L., 2015, Permian and Triassic sedimentation in the central Transantarctic mountains, southern Victoria Land and Northern Victoria Land: a south polar view of Gondwanan during the Paleozoic–Mesozoic transition, The 21st Internation Symposium on Polar Science: Polar Region as a Key Observatory for the Changing Globe and Beyond: Incheon, Republic of Korea, Korea Polar Institute.

ISBELL, J.L., GELHAR, G.A., AND SEEGERS, G.M., 1997a, Reconstruction of preglacial topography using a postglacial flooding surface: Upper Paleozoic deposits, central Transantarctic Mountains, Antarctica: Journal of Sedimentary Research, v. 67, p. 264–273.

ISBELL, J.L., SEEGERS, G.M., AND GELHAR, G.A., 1997b, Upper Paleozoic glacial and postglacial deposits, central Transantarctic Mountains, Antarctica, *in* Martini, I.P., ed., Late Glacial and Postglacial Environmental Changes: Quaternary, Carboniferous–Permian, and Proterozoic: Oxford, U.K., Oxford University Press, p. 230–242.

ISBELL, J.L., MILLER, M.F., BABCOCK, L.E., AND HASIOTIS, S.T., 2001, Ice-marginal environment and ecosystem prior to initial advance of the late Paleozoic ice sheet in the Mount Butters area of the central Transantarctic Mountains, Antarctica: Sedimentology, v. 48, p. 953–970.

ISBELL, J.L., COLE, D.I., AND CATUNEANU, O., 2008a, Carboniferous–Permian glaciation in the main Karoo Basin, South Africa: stratigraphy, depositional controls, and glacial dynamics, *in* Fielding, C.R., Frank, T.D., and Isbell, J.L., eds., Resolving the Late Paleozoic Ice Age in Time and Space: Geological Society of America, Special Publication 441, p. 71–82.

ISBELL, J.L., FRAISER, M.L., AND HENRY, L.C., 2008b, Examining the complexity of environmental change during the late Paleozoic and early Mesozoic: Palaios, v. 23, p. 267–269.

ISBELL, J.L., KOCH, Z.J., SZABLEWSKI, G.M., AND LENAKER, P.A., 2008c, Permian glacigenic deposits in the Transantarctic Mountains, Antarctica, *in* Fielding, C.R., Frank, T.D., and Isbell, J.L., eds., Resolving the Late Paleozoic Ice Age in Time and Space: Geological Society of America, Special Publication 441, p. 59–70.

ISBELL, J.L., HENRY, L.C., GULBRANSON, E.L., LIMARINO, C.O., FRAISER, M.L., KOCH, Z.J., CICCIOLI, P.L., AND DINEEN, A.A., 2012, Glacial paradoxes during the late Paleozoic ice age: evaluating the equilibrium line altitude as a control on glaciation: Gondwana Research, v. 22, p. 1–19.

JORDAN, T.A., FERRACCIOLI, F., ARMADILLO, E., AND BOZZO, E., 2013, Crustal architecture of the Wilkes Subglacial Basin in East Antarctica, as revealed fromairborne gravity data: Tectonophysics, v. 585, p. 196–206.

KESSLER, T.C., KLINT, K.E.S., NILSSON, B., AND BJERG, P.L., 2012, Characterization of sand lenses embedded in tills: Quaternary Science Reviews, v. 53, p. 55–71.

KOCH, Z.J., 2010, reevaluation of the late Paleozoicglacigenic deposits of the Pagoda Formation at Tillite Glacier, central Transanatarctic Mountains, Antarctica [Ph.D. Thesis]: University of Wisconsin–Milwaukee, Milwaukee, 145 p.

KOCH, Z.J., AND ISBELL, J.L., 2013, Processes and products of grounding-line fans from the Permian Pagoda Formation, Antarctica: insight into glacigenic conditions in polar Gondwana: Gondwana Research, v. 24, p. 161–172.

KURJANSKI, B., REA, B.R., SPAGNOLO, M., CORNWELL, D.G., HOWELL, J., AND ARCHER, S., 2020, A conceptual model for glaciogenic reservoirs: from landsystems to reservoir architecture: Marine and Petroleum Geology, v. 115, 104205.

LANDVIK, J.Y., ALEXANDERSON, H., HENRIKSEN, M., AND INGÓLFSSON, Ó., 2014, Landscape imprints of changing glacial regimes during ice-sheetbuild-up and decay: a conceptual model from Svalbard: Quaternary Science Reviews, v. 92, p. 258–268.

LAWSON, D.E., 1979, Sedimentological analysis of the western terminus region of the Matanuska Glacier, Alaska: Hanover, New Hampshire, U.S. Army, Cold Regions Research and Engineering Laboratory, 122 p.

LAWVER, L.A., DALZIEL, I.W.D., NORTON, I.O., AND GAHAGAN, L.M., 2011, The Plates 2011 Atlas of Plate Reconstructions (500 Ma to Present Day): University of Texas, Technical Report 198, 189 p.

LENAKER, P.A., 2002, Sedimentology of Permian glacial deposits in the Darwin Glacier region, Antarctica [M.S. Thesis]: University of Wisconsin–Milwaukee, 173 p.

LICHT, K.J., DUNBAR, N.W., ANDREWS, J.T., AND JENNINGS, A.E., 1999, Distinguishing subglacial till and glacial marine diamictons in the western Ross Sea, Antarctica: implications for a last glacial maximum grounding line: Geological Society of America, Bulletin, v. 111, p. 91–103.

LIMARINO, C.O., ALONSO-MURUAGA, P.J., CICCIOLI, P.L., LOINAZE, V.S.P., AND CÉSARI, S,N., 2014, Stratigraphy and palynology of a late Paleozoic glacial paleovalley in the Andean Precordillera, Argentina: Palaeogeography, Palaeoclimatology, Palaeoecology, v. 412, p. 223–240.

LINDBÄCK, K., AND PETTERSSON, R., 2015, Spectral roughness and glacial erosion of a land-terminating section of the Greenland Ice Sheet: Geomorphology, v. 238, p. 149–159.

LINDSAY, J.F., 1969, Stratigraphy and sedimentation of Lower Beacon rocks in the central Transantarctic Mountains, Antarctica: Institute of Polar Studies, Report 33: Research Foundation and the Institute of Polar Studies, The Ohio State University, 58 p.

LINDSAY, J.F., 1970a, Depositional environment of Paleozoic glacial rocks in the central Transantarctic Mountains: Geological Society of America, Bulletin, v. 81, p. 1149–1172.

LINDSAY, J.F., 1970b, Paleozoic cave deposit in the central Transantarctic Mountains: New Zealand Journal of Geology and Geophysics, v. 13, p. 1018–1023.

LISITZIN, A.P., 2002, Sea-Ice and Iceberg Sedimentation in the Ocean: Berlin, Springer-Verlag, 800 p.

LONG, W.E., 1964a, The stratigraphy of the Horlick Mountains, *in* Adie, R.J., ed., International Symposium on Antarctic Geology: Amsterdam, North Holand Publishing, p. 352–363.

LONG, W.E., 1964b, The stratigraphy of the Ohio Range, Antarctica [Ph.D. Thesis]: The Ohio State University, Columbus, Ohio, 340 p.

LONG, W.E., MCLELL, D., COLLINSON, J.W., AND ELLIOT, D.H., 2008–2009, Geology of the Nilsen Plateau, Queen Maud Mountains, Transantarctic Mountains: Terra Antarctica, v. 15, p. 239–253.

LØNNE, I., 1995, Sedimentary facies and depositional architecture of ice-contact glaciomarine systems: Sedimentary Geology, v. 98, p. 13–43.

LØNNE, I., NEMEC, W., BLIKRA, L.H., AND LAURITSEN, T., 2001, Sedimentary architecture and dynamic stratigraphy of a marine ice-contact system: Journal of Sedimentary Research, v. 71, p. 922–943.

LÓPEZ-GAMUNDÍ, O., LIMARINO, C.O., ISBELL, J.L., PAULS, K.N., CÉSARI, S.N., AND MURUAGA, P.A., 2021, The Late Paleozoic Ice Age along the southwestern margin of Gondwana: facies models, age constraints, correlation and sequence stratigraphic framework: Journal of South American Earth Sciences, v. 107, 103056.

MARCOS, P., GREGORI, D.A., BENEDINI, L., BARROS, M., STRAZZERE, L., AND PIVETTE, C.P., 2018, Pennsylvanian glacimarine sedimentation in the Cushamen Formation, western North Patagonian Massif: Geoscience Frontiers, v. 9, p. 485–504.

MARTIN, H., 1981, The late Palaeozoic Gondwana glaciation: Geologische Rundschau, v. 70, p. 480–496.

MARTIN, J.R., REDFERN, J., HORSTWOOD, M.S.A., MORY, A.J., AND WILLIAMS, B.P.J., 2019, Detrital zircon age and provenance constraints on late Paleozoic ice-sheet growth and dynamics in Western and Central Australia: Australian Journal of Earth Sciences, v. 66, p. 183–207.

MASOOD, K.R., TAYLOR, T.N., HORNER, T., AND TAYLOR, E.L., 1994, Palynology of the Mackellar Formation (Beacon Supergroup) of East Antarctica: Review of Palaeobotany and Palynology, v. 83, p. 329–337.

MATSCH, C.L., AND OJAKANGAS, R.W., 1991, Comparison in depositional style of "polar" and "temperate" glacial ice: late Paleozoic Whiteout Conglomerate (West Antarctica) and late Proterozoic Mineral Fork Formation (Utah), *in* Anderson, J.B., and Ashley, G.M., eds., Glacial Marine Sedimentation: Paleoclimatic Significance: Geological Society of America, Special Publication 261, p. 191–206.

MATSCH, C.L., AND OJAKANGAS, R.W., 1992, Stratigraphy and sedimentology of the Whiteout Conglomerate: a late Paleozoic glacigenic sequence in the Ellsworth Mountains, West Antarctica, *in* Webers, G.F., Craddock, G.F., and Splettstoesser, J.F., eds., Geology of the Ellsworth Mountains, Antarctica: Geological Society of America, Memoir 170, p. 37–62.

MCGREGOR, V.R., AND WADE, F.A., 1969, Geologic Map of Antarctica, Western Queen Maud Mountains: American Geographical Society of New York, Sheet 16.

MCKAY, R., BROWNE, G., CARTER, L., COWAN, E., DUNBAR, G., KRISSEK, L., NAISH, T., POWELL, R., REED, J., TALARICO, F., AND WILCH, T., 2009, The stratigraphic signature of the late Cenozoic Antarctic Ice Sheets in the Ross Embayment: Geological Society of America, Bulletin, v. 121, p. 1537–1561.

MILLER, J.M.G., 1989, Glacial advance and retreat sequences in a Permo-Carboniferous section, central Transantarctic Mountains: Sedimentology, v. 36, p. 419–430.

MINSHEW, V.H., 1967, Geology of the Scott Glacier and Wisconsin Range areas, central Transantarctic Mountains, Antarctica [Ph.D. Thesis]: The Ohio State University, 268 p.

MIRSKY, A., 1969, Geologic Map of Antarctica, Ohio Range to Liv Glacier: American Geographical Society, Sheet 17.

MONCREIFF, A.C.M., 1989, Classification of poorly sorted sediments: Sedimentary Geology, v. 65, p. 191–194.

MONTAÑEZ, I.P., AND POULSEN, C.J., 2013, The late Paleozoic ice age: an evolving paradigm: Annual Review of Earth and Planetary Sciences, v. 41, p. 1–28.

MONTAÑEZ, I., AND SOREGHAN, G.S., 2006, Earth's fickle climate: lessons learned from deep-time ice ages: Geotimes, v. 51, p. 24–27.

MONTAÑEZ, I.P., TABOR, N.J., NIEMEIER, D., DIMICHELE, W.A., FRANK, T.D., FIELDING, C.R., ISBELL, J.L., BIRGENHEIER, L.P., AND RYGEL, M.C., 2007, CO_2-forced climate and vegetation instability during late Paleozoic deglaciation: Science, v. 315, p. 87–91.

MORY, A.J., MARTIN, J.R., AND REDFERN, J., 2008, A review of Permian–Carboniferous glacial deposits in Western Australia, *in* Fielding, C.R., Frank, T.D., and Isbell, J.L., eds., Resolving the Late Paleozoic Ice Age in Time and Space: Geological Society of America, Special Publication 441, p. 29–40.

MULDER, T., AND ALEXANDER, J., 2001, The physical character of subaqueous sedimentary density flows and their deposits: Sedimentology, v. 48, p. 269–299.

MURRAY, K.T., MILLER, M.F., AND BOWSER, S.S., 2013, Depositional processes beneath coastal multi-year sea ice: Sedimentology, v. 60, p. 391–410.

NOAA, 2019, NCEI Geomagnetic Calculators, National Geophysical Data Center, National Oceanic and Atmospheric Administration, NOAA's National Centers for Environmental Information (NCEI), formerly the National Geophysical Data Center, and the collocated World Data Service for Geophysics, operated by NOAA/NESDIS/NCEI.

OJAKANGAS, R.W., AND MATSCH, C.L., 1981, The late Paleozoic Whiteout Conglomerate: a glacial and glaciomarine sequence in the Ellsworth Mountains, West Antarctica, *in*

Hambrey, M.J., and Harland, W.B., eds., Earth's pre-Pleistocene Glacial Record: Cambridge, Cambridge University Press, p. 241–244.

Partin, C.A., and Sadler, P.M., 2016, Slow net accumulation sets snowball Earth apart from all younger glacial episodes: Geology, v. 44, p. 1019–1022.

Pauls, K.N., 2014, Sedimentology and paleoecology of fossil-bearing, high-latitude marine and glacially influenced desposits in the Tepuel Basin, Patagonia, Argentina [M.S. Thesis]: University of Wisconsin–Milwaukee.

Posamentier, H.W., and Martinsen, O.J., 2011, The character and genesis of submarine mass-transport deposits: insights from outcrop and 3D seismic data, *in* Shipp, R.C., Weimer, P., and Posamentier, H.W., eds., Mass-Transport Deposits in Deepwater Settings: Society for Sedimentary Geology, Special Publication 96, p. 7–38.

Powell, R.D., 1990, Glacimarine processes at grounding-line fans and their growth to ice contact deltas, *in* Dowdeswell, J.A., and Scourse, J.D., eds., Glacimarine Environments: Processes and Sediments: Geological Society of London, Special Publication 53, p. 53–73.

Powell, R.D., 1991, Grounding-line systems as second-order controls on fluctuations of tidewater termini of temperate glaciers, *in* Anderson, J.B., and Ashley, G.M., eds., Glacial Marine Sedimentation: Paleoclimatic Significance: Geological Society of America, Special Publication 261, p. 75–93.

Powell, R.D., and Alley, R.B., 1997, Grounding-line systems: processes, glaciological inferences and the stratigraphic record, *in* Barker, P.F., and Cooper, A.C., eds., Geology and Siesmic Stratigraphy of the Antarctic Margin, 2: American Geophysical Union, Antarctic Research Series 71, p. 169–187.

Powell, R.D., and Cooper, J.M., 2002, A glacial sequence stratigraphic model for temperate, glaciated continental shelves: Geological Society, Special Publication 203, p. 215–244.

Powell, R., and Domack, E., 2002, Modern glaciomarine environments, *in* Menzies, J., ed., Modern and Past Glacial Environments: Oxford, Butterworth-Heinemann, p. 361–389.

Powell, R.D., and Molnia, B.F., 1989, Glacimarine sedimentary processes, facies and morphology of the south-southeast Alaska shelf and fjords: Marine Geology, v. 85, p. 359–390.

Raymond, A., and Metz, C., 2004, Ice and its consequences: glaciation in the late Ordovician, Late Devonian, Pennsylvanian–Permian, and Cenozoic compared: Journal of Geology, v. 112, p. 655–670.

Reineck, H.E., and Singh, I.B., 1980, Depositional Sedimentary Environments: Berlin, Springer-Verlag, 551 p.

Rocchi, S., Bracciali, L., Di Vincenzo, G., Gemelli, M., and Ghezzo, C., 2011, Arc accretion to the early Paleozoic Antarctic margin of Gondwana in Victoria Land: Gondwana Research, v. 19, p. 594–607.

Rodrigues, M.C.N., Trzakos, B., Alsop, G.I., and Vesely, F.F., 2019, Making a homogenite: an outcrop perspective into the evolution of deformation within mass-transport deposits: Marine and Petroleum Geology, v. 112, 104033.

Rosa, E.L.M., and Isbell, J.L., 2021, Late Paleozoic glaciation: Reference Module in Earth Systems and Environmental Sciences, Elsevier, p. 534–545.

Rosa, E.L.M., Vesely, F.F., and França, A.B., 2016, A review on late Paleozoic ice-related erosional landforms in the Paraná Basin: origin and paleogeographical implications: Brazilian Journal of Geology, v. 46, p. 147–166.

Rose, P., Byerley, G., Vaughan, O., Cater, J., Rea, B.R., Spagnolo, M., and Archer, S., 2018, Aviat: a Lower Pleistocene shallow gas hazard developed as a fuel gas supply for the Forties Field, *in* Bowman, M., and Levell, B., eds., Petroleum Geology of NW Europe: 50 Years of Learning: Geological Society of London, Petroleum Geology Conference Series 8, Proceedings, p. 485–505.

Rosenblume, J.A., and Powell, R.D., 2019, Glacial sequence stratigraphy of ANDRILL-1B core reveals adynamic subpolar Antarctic Ice Sheet in Ross Sea during the late Miocene: Sedimentology, v. 66, p. 2072–2097.

Rust, I.C., 1975, Tectonic and sedimentary framework of Gondwana basins in southern Africa, *in* Campbell, K.S.W., ed., Gondwana Geology: Canberra, Australian National University Press, p. 537–564.

Rygel, M.C., Fielding, C.R., Frank, T.D., and Birgenheier, L.P., 2008, The magnitude of late Paleozoic glacioeustatic fluctuations: a synthesis: Journal of Sedimentary Research, v. 78, p. 500–511.

Seegers, G.M., 1996, Sedimentology of the Permian Mackellar Formation, Central Transantarctic Mountains, Antarctica [M.S. Thesis]: University of Wisconsin–Milwaukee, 106 p.

Seegers-Szablewski, G., and Isbell, J.L., 1998, Stratigraphy and depositional environments of Lower Permian post-glacial rocks exposed between the Byrd and Nimrod Glaciers, Antarctica: Journal of African Earth Sciences, v. 27, p. 175–176.

Shaw, J., 2016, Paraglacial landscapes in St George's Bay, Newfoundland, Canada, *in* Dowdeswell, J.A., Canals, M., Jakobsson, B.J., Todd, B.J., Dowdeswell, E.K., and Hogan, K.A., eds., Atlas of Submarine Glacial Landforms: Modern, Quaternary and Ancient: Geological Society of London, Memoir 46, p. 97–98.

Sheppard, K., Bell, T., and Liverman, D.G.E., 2000, Late Wisconsinan stratigraphy and chronology at Highlands, southern St. George's Bay, southwest Newfoundland: Quaternary International, v. 68–71, p. 275–283.

Sobiesiak, M.S., Kneller, B., Alsop, G.I., and Milana, J.P., 2018, Styles of basal interaction beneath mass transport deposits: Marine and Petroleum Geology, v. 98, p. 629–639.

Soreghan, G.S., Soreghan, M.J., and Heavens, N.G., 2019, Explosive volcanism as a key driver of the late Paleozoic ice age: Geology, v. 47, p. 600–604.

Survis, S.R., 2015, Sedimentology and stratigraphy of high-latitude, glacigenic deposits from the Late Paleozoic Ice Age in the Tepuel–Genoa Basin, Patagonia, Argentina [M.S. Thesis]: University of Wisconsin–Milwaukee, 104 p.

Svendsen, J.I., and Mangerud, J., 1997, Holocene glacial and climatic variations on Spitsbergen, Svalbard: The Holocene, v. 7, p. 45–57.

Tedesco, J., Cagliari, J., Coitinho, J.D.R., Lopes, R.D.C., and Lavina, E.L.C., 2016, Late Paleozoic paleofjord in the southernmost Parana Basin (Brazil): geomorphology and sedimentary fill: Geomorphology, v. 269, p. 203–214.

Thomas, G.S.P., and Chiverrell, R.C., 2006, A model of subaqueous sedimentation at the margin of the Late Midlandian Irish Ice Sheet, Connemara, Ireland, and its implications for regionally high isostatic sea levels: Quaternary Science Reviews, v. 25, p. 2868–2893.

Thomas, G.S.P., and Connell, R.J., 1985, Iceberg drop, dump, and grounding structures from Pleistocene glacio-lacustrine sediments, Scotland: Journal of Sedimentary Petrology, v. 55, p. 243–249.

Veevers, J.J., and Tewari, R.C., 1995, Gondwana master basin of Peninsular India between Tethys and the interior of the Gondwanaland province of Pangea: Geological Society of America, Memoir 187, 72 p.

Veevers, J.J., Powell, C.M., Collinson, J.W., and López-Gamundí, O.R., 1994, Synthesis, *in* Veevers, J.J., and Powell, C.M., eds., Permian–Triassic Pangean basins and foldbelts along the Panthalassan Margin of Gondwanaland: Geological Society of America, Memoir 184, p. 331–353.

Vesely, F., and Assine, M.L., 2014, Ice-keel scour marks in the geologic record: evidence from Carboniferous soft-sediment striated surfaces in the Paraná Basin, southern Brazil: Journal of Sedimentary Research, v. 84, p. 26–39.

Vesely, F.F., Rodrigues, M.C.N.L., Da Rosa, E.L.M., Amato, J.A., Trzaskos, B., Isbell, J.L., and Fedorchuk, N.D., 2018, Recurrent emplacement of non-glacial diamictite during the late Paleozoic ice age: Geology, v. 46, p. 615–618.

Visser, J.N.J., 1987, The palaeogeography of part of southwestern Gondwana during the Permo-Carboniferous glaciation: Palaeogeography, Palaeoclimatology, Palaeoecology, v. 61, p. 205–219.

Visser, J.N.J., 1994, The interpretation of massive rain-out and debris-flow diamictites from the glacial marine environment, *in* Deynoux, M., Miller, J.M.G., Domack, E.W., Eyles, N., Fairchild, I.J., and Young, G.M., eds., Earth's Glacial Record: Cambridge, Cambridge University Press, p. 83–94.

Visser, J.N.J., 1997, A review of the Permo-Carboniferous glaciation in Africa, *in* Martini, I.P., ed., Late Glacial and Postglacial Environmental Changes: Quaternary, Carboniferous–Permian, and Proterozoic: Oxford, U.K., Oxford University Press, p. 169–191.

Visser, J.N.J., Loock, J.C., and Colliston, W.P., 1987, Subaqueous outwash fan and esker sandstones in the Permo-Carboniferous Dwyka Formation of South Africa: Journal of Sedimentary Petrology, v. 57, p. 467–478.

Vizán, H., Prezzi, C.B., Geuna, S.E., Japas, M.S., Renda, E.M., Franzese, J., and Van Zele, M.A., 2017, Paleotethys slab pull, self-lubricated weak lithospheric zones, poloidal and toroidal plate motions, and Gondwana tectonics: Geosphere, v. 13, 1541–1554.

Waugh, B.J., 1988, Sedimentology and petrology of sandstones from the Permo-Carboniferous Pagoda Formation, central Transantarctic Mountains, Antarctica [M.S. Thesis]: Vanderbilt University, 146 p.

Wopfner, H., 2012, Late Palaeozoic–Early Triassic deposition and climates between Samfrau and Tethys: a review, *in* Gąsiewicz, M., and Słowakiewicz, M., eds., Paleozoic Climate Cycles: Their Evolutionary and Sedimentological Impact: Geological Society of London, Special Publication 376, p. 5–32.

Wright, R., and Anderson, J.B., 1982, The importance of sediment gracity flow to sediment transport and sorting in a glacial marine environment, Eastern Weddell Sea, Antarctica: Geological Society of America, Bulletin, v. 93, p. 951–963.

Received 13 January 2021; accepted 13 April 2021.

Queries for sedp-91-06-03

This article has been typeset from the submitted materials. Check proofs carefully for conversion or other inadvertent errors. Please follow the Allen Press Guide to PDF Annotation when marking revisions. Do not edit the PDF directly.

If present, queries will be listed below with corresponding numbers in the margins or may appear as PDF comments addressed to the author or editor. If a correction is desired in response to a query, mark the necessary changes directly in the proof using the appropriate annotation tool. If no change is desired, no action is necessary in response.